The Canadian Mineralogist
Vol. 48, pp. 1081-1107 (2010)
DOI: 10.3749/canmin.48.5.1081

THE CRYSTAL CHEMISTRY OF COSALITE BASED ON NEW ELECTRON-MICROPROBE DATA AND SINGLE-CRYSTAL DETERMINATIONS OF THE STRUCTURE

DAN TOPA[§]

Department of Materials Research and Physics, Paris–Lodron University of Salzburg, Hellbrunnerstrasse 34, A–5020, Salzburg, Austria

EMIL MAKOVICKY

Department of Geography and Geology, University of Copenhagen, Østervoldgade 10, DK–1350 Copenhagen, Denmark

ABSTRACT

Crystal-structure refinements done on six samples of cosalite with different types and degrees of copper and silver substitutions, as well as electron-microprobe studies of 33 different samples of cosalite, both enlarged and clarified the spectrum of cation substitutions and the crystal chemistry of this species. The Ag + Bi ↔ 2Pb scheme of substitution acts at the structural site *Me*1. The 2(Cu + Ag) ↔ Pb scheme is a result of two combined mechanisms: creation of vacancies in the Bi-containing octahedral site *Me2* accompanied by a progressive occupancy of two triangular faces of this octahedron by Cu + Ag [*i.e.*, Bi ↔ 2(Cu + Ag)], which is combined with progressive replacement of Pb in the adjacent *Me*1 octahedron by Bi; their combination gives the resulting closely followed chemical relationship. The structural mechanism of the 3Cu ↔ Bi substitution observed in thin zones in cosalite from Felbertal remains unknown. Cosalite offers a unique case of solid solution based on a combined omission – interstitial insertion substitution.

Keywords: cosalite, sulfosalt, crystal structure, crystal chemistry, mechanisms of substitution.

SOMMAIRE

Nous avons effectué des affinements de la structure cristalline de six échantillons de cosalite montrant des différents types et degrés de substitution impliquant le cuivre et l'argent, ainsi que des analyses avec une microsonde électronique de 33 échantillons différents de cosalite, ce qui a considérablement élargi et éclairci le spectre de substitutions cationiques et la cristallochimie de cette espèce. Le schéma de substitution Ag + Bi ↔ 2Pb affecte le site structural *Me*1. Le schéma 2(Cu + Ag) ↔ Pb est le résultat de deux mécanismes combinés: création de lacunes au site octaédrique *Me2* contenant le Bi, accompagné de l'occupation progressive de deux faces triangulaires de cet octaèdre par Cu + Ag [*i.e.*, Bi ↔ 2(Cu + Ag)], qui à son tour est associée au remplacement progressif de Pb dans l'octaèdre adjacent *Me*1 par le Bi. Leur combinaison mène à une relation chimique serrée. Le mécanisme structural de la substitution structurale 3Cu ↔ Bi observée dans les liserés de grains de cosalite à Felbertal demeure méconnu. La cosalite offre un cas unique de solution solide fondée sur une substitution combinant une omission et une insertion interstitielle.

(Traduit par la Rédaction)

Mots-clés: cosalite, sulfosel, structure cristalline, cristallochimie, mécanismes de substitution.

§ *E-mail address*: dan.topa@sbg.ac.at

Introduction and Previous Investigations

Cosalite belongs to the long-known "classical" lead–bismuth sulfosalts. It was analyzed and described by Genth (1885) from the Cosala mine, Sinaloa, Mexico, but it is now known from a large number of occurrences. Its composition is usually quoted as $Pb_2Bi_2S_5$, although "minor amounts" of Cu, Ag and Fe (Palache *et al.*1966) have been known in cosalite since the first analyses of this mineral were made. Antimony-containing cosalite has been described by Lee *et al.* (1993), Lee & Park (1995), and Cook (1997); selenium-rich cosalite has been reported by Mozgova *et al.* (1992). Ciobanu *et al.* (2009) studied trace gold contents in cosalite by ICP–MS.

Berry (1939) determined the unit cell and space group of the mineral, and Weitz & Hellner (1960) performed the first determination of its structure. Their results were refined substantially by Srikrishnan & Nowacki (1974) using, as a novelty at that time, data obtained on a single-crystal diffractometer. They determined the unit-cell parameters to be *a* 23.890(5), *b* 4.057(1), *c* 19.098(4) Å, space group *Pnma*, on the basis of systematic extinctions and intensity statistics. They defined four independent Bi positions, four Pb sites (one of which, a trigonal-prismatic site, has an occupancy of only 0.5, at variance with the chemical formula) and ten different sulfur sites (two of which have an occupancy of 0.5 as well). They also found a distorted-tetrahedral Cu site with an occupancy of only 0.12. The final *R* value was 9.6%, and no comments were made on the half-occupied sites. Cosalite belongs to the group of sulfosalts based on rod-type building blocks (Makovicky 1981, 1989, 1993).

Macíček (1986) addressed the question of Cu and Ag substitution in cosalite by structural analysis of a specimen from the Strandza Mountains, Bulgaria, with the empirical formula given as $Ag_{0.12}Cu_{0.5}Pb_{3.54}Bi_4S_{10}$. He re-interpreted some of the Pb and Bi site assignments, especially the position Pb2 of Srikrishnan & Nowacki (1974), which he described as an approximately three-quarter-occupied (Bi + Ag) site *Me*3. He also found about one-third-occupied Cu sites in the triangular walls of the *Me*3 octahedra. The unit-cell parameters of his specimen are *a* 23.860, *b* 4.055, *c* 19.072 Å; the resulting *R* value was 3%. Wulf (1988, 1995) investigated cosalite of unspecified composition from Bergell, Switzerland by means of Δ synthesis and bichromatic least-squares refinement, using a combination of X-ray wavelengths, 0.953 Å (the Pb-*LIII* absorption edge) and 0.988 Å (a reference wavelength). He reassigned the lead site Pb2 of Srikrishnan & Nowacki (1974) as bismuth, and their Bi3 site as lead. There is a full correspondence between Wulf's and Macíček's site assignment. However, Wulf did not seem to be aware of the partial occupancy of the "Pb2"site and of the Cu,Ag atoms surrounding it; this may have caused problems in interpretation, especially in his results of the bichromatic least-squares refinement.

An electron-diffraction and HRTEM investigation of (Cu,Ag)-rich cosalite from Ivigtut, Greenland, with a chemical formula $Cu_{1.2}Ag_{0.9}Pb_{6.7}Bi_{8.2}S_{20}$, originally described by Karup-Møller (1977), was performed by Pring & Etschmann (2002). In the strong-intensity areas of the (*hk*0) plane of the reciprocal lattice, they found pairs of satellites deviating by several degrees from the [010]* direction (in Srikrishnan's & Nowacki's orientation) and, in the HRTEM photograph down the 4 Å zone, a wavy modulation along the corresponding direction. They ascribed these phenomena to a combined compositional and displacive modulation coupled with the ordering of (Ag,Pb,Bi) and Cu and an associated structural relaxation.

Skowron & Brown (1990) determined the structure of $Pb_4Sb_4Se_{10}$, which is isotypic with (ideal) cosalite. By using bond-valence calculations, they determined mixed (Pb,Sb) occupancy for all cation sites with the exception of the trigonal-prismatic Pb3 and Pb4 sites.

Karup-Møller (1977) dealt with substitutions in cosalite. From his electron-microprobe data, he found an inverse correlation of (Ag + Cu) with Pb, an absent-to-positive correlation between (Ag + Cu) and Bi, and a very weak increase in Cu accompanying a sizable increase in Ag. On the basis of these results, he proposed the $Pb^{2+} \leftrightarrow 2(Ag,Cu)^{+}$ substitution as the probable mechanism, with one monovalent atom substituting for Pb and the other, Cu^{+}, assumed to be tetrahedrally coordinated and interstitial to the parent structure. He postulated that silver-rich cosalite requires Cu for stabilization and that a substitution $2Bi^{3+} + \square \leftrightarrow 3Pb^{2+}$ might play a role as well. Moëlo *et al.* (2008) suggested $Bi^{3+} + \square \leftrightarrow Pb^{2+} + Cu^{+}$ as another possible mechanism present in cosalite.

Sugaki *et al.* (1982) synthesized cosalite in the dry system Cu–Pb–Bi–S at 400°C and also under hydrothermal conditions. They gave its composition as $CuPb_7Bi_8S_{20}$, with unit-cell parameters *a* 19.134, *b* 23.804, *c* 4.059 Å, space group *Pbnm*. In their formula, they assumed Cu^{2+} instead of monovalent copper.

On the one hand, these investigations defined the fundamental scheme for the crystal structure of cosalite but, on the other, they revealed a complexity of substitution mechanisms in this mineral, both from the compositional and the structural point of view. Most of them were performed in a single sample or on a small number of them. Thus, a study of a broad spectrum of chemical compositions of cosalite was desirable, connected with the maximum possible number of precise determination of the structure. One purpose of this study is to do just that and, if possible, to come up with a final answer on the compositional limits, mechanisms of substitution and structural details on this fairly common, compositionally complex sulfosalt.

EXPERIMENTAL

Chemical analysis

Quantitative chemical analyses were performed with a JEOL JXA–8600 electron microprobe controlled by LINK–*eXL* system, WDS mode, operated at 25 kV, and 30 nA, 20 s counting time for peaks and 7 s for background, at the University of Salzburg. The following natural and synthetic standards and X-ray lines were used: chalcopyrite (Cu$K\alpha$, Fe$K\alpha$), galena (Pb$L\alpha$), stibnite (Sb$L\alpha$), Bi_2S_3 (Bi$L\alpha$, S$K\alpha$), Bi_2Se_3 (Se$K\alpha$), CdTe (Cd$L\beta$, Te$L\alpha$), and pure metal for Ag$L\alpha$. Beside Pb, Bi and S as major constituent components, Cu and Ag are invariably present in various amounts. The raw data were corrected with the on-line ZAF–4 procedure. Standard deviations (error in wt.%) of elements sought in cosalite are: Bi and Pb 0.16, Ag 0.08, Sb 0.07, Cd and S 0.06, Cu and Fe 0.02. Three to five point-analyses obtained from a homogeneous grain or an individual phase in an aggregate were averaged. Chemical data for the cosalite occurrences studied and for the materials structurally investigated are compiled in Tables 1 and 2, respectively.

Single-crystal X-ray diffraction

Fragments of cosalite of irregular shape from (1) Felbertal, (2) Habachtal, (3) Altenberg, (4) Ocna de Fier (Romania), (5) Erzwiess, and (6) Schareck [all localities, except no. 4, are situated in the Hohe Tauern (Tauern Window), Salzburg Province, Austria] were measured on a Bruker AXS diffractometer (at the University of Salzburg, except for specimen no. 1, measured at the University of Copenhagen), equipped with a CCD area detector using graphite-monochromated Mo$K\alpha$ radiation. Experimental settings for the cosalite materials studied are listed in Tables 3 and 4. The SMART (Bruker AXS, 1998a) system of programs was used for unit-cell determination and data collection, SAINT + (Bruker AXS, 1998b) for the calculation of integrated intensities, and XPREP (Bruker AXS, 1998c) for the empirical absorption-correction based on pseudo-Ψ scans. The centrosymmetric space-group *Pnma*, proposed by the XPREP program, was chosen and is consistent with the orthorhombic symmetry of the lattices and intensity statistics. The structure model of cosalite was verified using direct methods (the program SHELXS of Sheldrick 1997a), which revealed most of the cation positions. In subsequent cycles of the refinement (the program SHELXL of Sheldrick 1997b), the additional atom-positions were verified by means of difference-Fourier syntheses. The structures were refined (the program SHELXL of Sheldrick 1997b) using the choice of asymmetric unit and atom labeling published by Srikrishnan & Nowacki (1974) as a starting input. Final fractional coordinates of atoms, as well as their isotropic and anisotropic displacement parameters in the refined structures, are listed in Table 5. Details of the assignment of the partly occupied positions and mixed cation sites will be given in the section on the description of the structure.

Selected *Me*–S bond distances are presented in Table 6, and selected geometrical parameters for individual coordination polyhedra, calculated with the IVTON program (Balić-Žunić & Vicković 1996), are given in Table 7. The tables of structure factors for the six cosalite specimens investigated may be obtained from the Depository of Unpublished Data, on the MAC website [document Cosalite CM48_1081]. With substitutions at some positions, vacancies at other positions, and occupancy of two different positions by a potential mixture of Cu and Ag in distinct proportions, it is practically impossible to achieve a full agreement between the microprobe data and structure refinement, especially where the contents of Ag or Cu, or of both cations, are low. A comparison of the models derived from, or used in, the structure refinement with electron-microprobe data is presented in Table 8.

THE COMPOSITION OF COSALITE

The large body of new electron-microprobe data on cosalite (Tables 1, 2) comprises the following categories: (1) material from the relatively Cu-rich samples from two ore deposits in Argentina (Id_1: A1 to A4 in Table 1, Fig.1a), (2) material from two deposits (Radhausberg and Goldzeche) in the Tauern Window of the Austrian Alps, Salzburg Province, Austria (Id_1: TW1 to TW9 in Table 1, Fig. 1a), concentrated along the line with 50 mol.% of (Bi + Sb), with very variable Cu contents, (3) material from various orebodies (K1–K7) in the Felbertal scheelite deposit, Tauern Window, Salzburg Province, Austria (Id_1: F1 to F11 in Table 1, Fig. 1b), that shows an extensive range of Ag and especially Cu substitution, (4) rims highly enriched in copper along fractures in cosalite from the K3 orebody of the Felbertal deposit (Id_1: F12 to F14 in Table 1, Fig. 1b), and (5) data from the six structurally analyzed specimens with a broad range of Cu and Ag substitution (no. 1 to no. 6 in Table 2, Fig. 1c).

In the structurally analyzed sample no. 1 from Felbertal, cosalite is associated with Ag-poor lillianite as well as galenobismutite. The Habachtal sample (no. 2) contains nuffieldite, galenobismutite and eclarite, *i.e.*, a (Cu,Ag)-poor association as well. No other sulfosalt accompanies free cosalite crystals in the vugs of carbonate gangue from Altenberg. Sample no. 4 from Ocna de Fier consists of massive cosalite in quartz. In the Erzwiess material (no. 5), cosalite coexists with the members of the pavonite and lillianite homologous series, whereas the Schareck sample (no. 6) is composed of (Cu,Ag)-containing galena that encloses aikinite, cosalite and (Cu,Ag)-rich neyite. Detailed information

TABLE 1. AVERAGE RESULTS OF ELECTRON-MICROPROBE ANALYSES OF COSALITE FROM VARIOUS OCCURRENCES

No.	NA	Cu	Ag	Fe	Pb	Cd	Bi	Sb	Te	S	Total	*ch*	*ev*	Pb*	CuAg*	Me^{XS}	Id_1	Id_2
1	13	0.82(3)	0.49(4)	-	39.75(30)	-	42.68(25)	0.112(1)	0.14(2)	16.24(9)	100.23(62)	0.12	0.11	7.72	0.61	0.33	A 1	g1
2	4	1.38(12)	1.88(7)	0.03(1)	36.78(39)	-	41.87(15)	1.10(8)	-	16.47(6)	99.51(46)	-0.43	-0.40	7.23	1.38	0.61	A 2	g1
3	13	2.08(7)	2.29(14)	-	34.67(26)	-	44.49(15)	-	0.09(7)	16.41(7)	100.03(33)	0.26	0.24	7.15	1.80	0.95	A 3	g1
4	3	2.39(11)	1.67(3)	0.09(1)	37.35(39)	-	39.78(15)	1.66(8)	-	16.61(6)	99.51(17)	-0.75	-0.70	-	-	0.95	A 4	g1
5	58	0.22(5)	0.46(9)	0.15(3)	40.62(30)	0.23(11)	40.93(45)	1.21(22)	0.09(6)	16.44(7)	100.34(42)	-0.05	-0.04	7.86	0.29	0.13	TW 1	g2
6	8	0.70(4)	1.34(14)	-	38.54(56)	-	43.05(17)	0.38(2)	-	16.37(5)	100.37(32)	0.18	0.17	7.67	0.72	0.40	TW 2	g2
7	8	0.44(2)	2.86(12)	0.06(1)	36.46(23)	0.23(3)	35.30(40)	7.04(35)	0.24(6)	17.23(7)	99.86(43)	-0.69	-0.62	7.46	0.83	0.29	TW 3	g2
8	11	1.04(2)	0.89(4)	-	38.87(20)	0.23(4)	41.75(16)	0.42(5)	-	16.32(7)	99.52(21)	-0.50	-0.46	7.45	0.96	0.40	TW 4	g2
9	7	1.07(3)	1.46(3)	-	38.26(21)	0.11(10)	42.87(28)	-	-	16.37(2)	100.14(15)	-0.43	-0.39	7.33	1.16	0.49	TW 5	g2
10	15	1.34(5)	1.42(14)	-	37.61(28)	-	43.34(21)	-	0.09(5)	16.37(8)	100.17(14)	-0.25	-0.23	7.33	1.23	0.56	TW 6	g2
11	6	1.02(6)	3.43(21)	0.08(2)	34.47(32)	0.33(7)	37.10(57)	6.23(55)	0.15(2)	17.20(9)	100.02(38)	0.02	0.02	7.37	1.27	0.64	TW 7	g2
12	24	1.36(3)	1.73(5)	-	36.49(21)	-	43.38(15)	-	-	16.27(7)	99.26(22)	-0.32	-0.29	7.29	1.29	0.59	TW 8	g2
13	7	1.79(4)	1.94(10)	-	36.53(16)	-	43.38(35)	-	-	16.42(5)	100.06(20)	-0.27	-0.25	7.10	1.69	0.80	TW 9	g2
14	8	0.22(5)	0.40(5)	0.14(5)	40.90(17)	-	40.54(28)	1.30(18)	-	16.36(4)	99.86(22)	0.05	0.05	7.89	0.25	0.14	F 1	g3
15	15	0.20(4)	0.46(4)	0.11(1)	40.26(14)	0.35(6)	42.36(21)	0.36(1)	-	16.42(5)	100.52(27)	-0.11	-0.10	7.86	0.26	0.11	F 2	g3
16	8	0.25(3)	0.74(7)	0.11(1)	39.34(23)	0.22(4)	42.43(26)	0.26(6)	-	16.27(5)	99.62(28)	-0.07	-0.06	7.82	0.34	0.16	F 3	g3
17	5	0.45(12)	0.76(3)	0.11(1)	38.89(51)	0.34(7)	43.44(10)	0.10(6)	-	16.45(3)	100.54(33)	-0.10	-0.09	7.78	0.42	0.20	F 4	g3
18	11	0.26(2)	1.22(7)	0.07(1)	38.47(10)	-	43.52(27)	-	-	16.31(4)	99.84(18)	-0.37	-0.33	7.73	0.42	0.14	F 5	g3
19	3	0.28(1)	1.48(4)	0.06(1)	37.45(10)	0.56(5)	44.08(8)	0.13(1)	-	16.45(2)	100.48(5)	0.17	0.15	7.79	0.44	0.24	F 6	g3
20	3	0.51(5)	1.56(5)	0.07(5)	36.87(33)	0.33(3)	44.08(19)	0.19(2)	-	16.39(7)	100.02(7)	0.14	0.13	7.74	0.57	0.31	F 7	g3
21	1	1.14	1.27	-	36.45	0.61	43.60	0.12	0.22	16.34	99.76	-0.19	-0.17	7.49	0.96	0.45	F 8	g3
22	36	1.09(6)	1.56(15)	-	37.91(23)	-	43.37(42)	0.20(12)	-	16.41(6)	100.53(47)	0.22	0.21	7.51	1.05	0.57	F 9	g3
23	118	1.49(23)	1.30(13)	-	36.34(34)	0.70(7)	43.41(39)	0.09(6)	0.17(5)	16.32(13)	99.81(58)	0.37	0.34	7.45	1.22	0.68	F10	g3
24	32	2.26(20)	1.24(14)	-	36.39(26)	0.59(12)	42.80(40)	0.10(5)	0.13(6)	16.36(13)	99.87(49)	0.34	0.31	7.17	1.79	0.96	F11	g3
25	7	4.00(5)	0.92(6)	-	36.42(19)	0.17(21)	41.13(23)	0.13(3)	0.12(5)	16.27(11)	99.16(31)	0.37	0.35	-	-	1.58	F12	g4
26	24	4.62(18)	0.91(13)	-	36.35(25)	-	40.43(30)	0.13(6)	0.11(6)	16.35(10)	99.10(34)	-0.15	-0.14	-	-	1.75	F13	g4
27	20	5.42(12)	0.88(7)	-	36.21(24)	-	40.58(18)	0.12(3)	0.11(4)	16.53(9)	99.91(43)	-0.29	-0.27	-	-	1.98	F14	g4

1)	$(Cu_{0.51}Ag_{0.18})_{\Sigma 0.69}(Fe_{0.00}Pb_{7.56}Cd_{0.00})_{\Sigma 7.56}(Bi_{8.04}Sb_{0.04})_{\Sigma 8.08}Te_{0.04}S_{19.96}$	or, after $Ag_s + Bi^{excess} \rightarrow 2Pb$	$(Cu_{0.51}Ag_{0.10})_{\Sigma 0.61}Pb_{7.72}Bi_8S_{20}$
2)	$(Cu_{0.85}Ag_{0.68})_{\Sigma 1.53}(Fe_{0.02}Pb_{6.91}Cd_{0.00})_{\Sigma 6.93}(Bi_{7.80}Sb_{0.35})_{\Sigma 8.15}Te_{0.00}S_{20.00}$		$(Cu_{0.85}Ag_{0.53})_{\Sigma 1.38}Pb_{7.23}Bi_8S_{20}$
3)	$(Cu_{1.26}Ag_{0.83})_{\Sigma 2.11}(Fe_{0.00}Pb_{6.53}Cd_{0.00})_{\Sigma 6.53}(Bi_{8.31}Sb_{0.00})_{\Sigma 8.31}Te_{0.03}S_{19.97}$		$(Cu_{1.26}Ag_{0.52})_{\Sigma 1.80}Pb_{7.15}Bi_8S_{20}$
4)	$(Cu_{1.45}Ag_{0.60})_{\Sigma 2.05}(Fe_{0.06}Pb_{6.96}Cd_{0.00})_{\Sigma 7.02}(Bi_{7.35}Sb_{0.53})_{\Sigma 7.88}Te_{0.00}S_{20.00}$		$(Cu_{1.45}Ag_{0.60})_{\Sigma 2.05}Pb_{7.02}Bi_{7.88}S_{20}$
5)	$(Cu_{0.14}Ag_{0.17})_{\Sigma 0.31}(Fe_{0.10}Pb_{7.64}Cd_{0.08})_{\Sigma 7.82}(Bi_{7.63}Sb_{0.39})_{\Sigma 8.02}Te_{0.03}S_{19.97}$		$(Cu_{0.14}Ag_{0.15})_{\Sigma 0.29}Pb_{7.86}Bi_8S_{20}$
6)	$(Cu_{0.43}Ag_{0.49})_{\Sigma 0.92}(Fe_{0.00}Pb_{7.29}Cd_{0.00})_{\Sigma 7.29}(Bi_{8.07}Sb_{0.12})_{\Sigma 8.19}Te_{0.00}S_{20.00}$		$(Cu_{0.43}Ag_{0.30})_{\Sigma 0.72}Pb_{7.67}Bi_8S_{20}$
7)	$(Cu_{0.26}Ag_{0.98})_{\Sigma 1.24}(Fe_{0.04}Pb_{6.53}Cd_{0.08})_{\Sigma 6.65}(Bi_{6.27}Sb_{2.14})_{\Sigma 8.41}Te_{0.07}S_{19.93}$		$(Cu_{0.26}Ag_{0.57})_{\Sigma 0.83}Pb_{7.47}Bi_8S_{20}$
8)	$(Cu_{0.64}Ag_{0.32})_{\Sigma 0.96}(Fe_{0.00}Pb_{7.37}Cd_{0.08})_{\Sigma 7.45}(Bi_{7.85}Sb_{0.13})_{\Sigma 7.98}Te_{0.00}S_{20.00}$		$(Cu_{0.64}Ag_{0.32})_{\Sigma 0.96}Pb_{7.45}Bi_8S_{20}$
9)	$(Cu_{0.66}Ag_{0.53})_{\Sigma 1.19}(Fe_{0.00}Pb_{7.23}Cd_{0.04})_{\Sigma 7.27}(Bi_{8.03}Sb_{0.00})_{\Sigma 8.03}Te_{0.00}S_{20.00}$		$(Cu_{0.66}Ag_{0.50})_{\Sigma 1.16}Pb_{7.33}Bi_8S_{20}$
10)	$(Cu_{0.83}Ag_{0.51})_{\Sigma 1.34}(Fe_{0.00}Pb_{7.11}Cd_{0.00})_{\Sigma 7.11}(Bi_{8.11}Sb_{0.00})_{\Sigma 8.11}Te_{0.03}S_{19.97}$		$(Cu_{0.83}Ag_{0.40})_{\Sigma 1.23}Pb_{7.99}Bi_8S_{20}$
11)	$(Cu_{0.60}Ag_{1.18})_{\Sigma 1.78}(Fe_{0.05}Pb_{6.19}Cd_{0.11})_{\Sigma 6.35}(Bi_{8.61}Sb_{1.90})_{\Sigma 8.51}Te_{0.04}S_{19.96}$		$(Cu_{0.60}Ag_{0.67})_{\Sigma 1.27}Pb_{7.37}Bi_8S_{20}$
12)	$(Cu_{0.84}Ag_{0.63})_{\Sigma 1.47}(Fe_{0.00}Pb_{6.94}Cd_{0.00})_{\Sigma 6.94}(Bi_{8.18}Sb_{0.00})_{\Sigma 8.18}Te_{0.00}S_{20.00}$		$(Cu_{0.84}Ag_{0.45})_{\Sigma 1.29}Pb_{7.29}Bi_8S_{20}$
13)	$(Cu_{1.10}Ag_{0.70})_{\Sigma 1.80}(Fe_{0.00}Pb_{6.89}Cd_{0.00})_{\Sigma 6.89}(Bi_{8.11}Sb_{0.00})_{\Sigma 8.11}Te_{0.00}S_{20.00}$		$(Cu_{1.10}Ag_{0.59})_{\Sigma 1.69}Pb_{7.10}Bi_8S_{20}$
14)	$(Cu_{0.14}Ag_{0.14})_{\Sigma 0.28}(Fe_{0.10}Pb_{7.74}Cd_{0.00})_{\Sigma 7.84}(Bi_{7.61}Sb_{0.42})_{\Sigma 8.03}Te_{0.00}S_{20.00}$		$(Cu_{0.14}Ag_{0.11})_{\Sigma 0.25}Pb_{7.89}Bi_8S_{20}$
15)	$(Cu_{0.12}Ag_{0.17})_{\Sigma 0.29}(Fe_{0.08}Pb_{7.59}Cd_{0.12})_{\Sigma 7.79}(Bi_{7.91}Sb_{0.12})_{\Sigma 8.03}Te_{0.00}S_{20.00}$		$(Cu_{0.12}Ag_{0.14})_{\Sigma 0.26}Pb_{7.86}Bi_8S_{20}$
16)	$(Cu_{0.16}Ag_{0.27})_{\Sigma 0.43}(Fe_{0.08}Pb_{7.49}Cd_{0.08})_{\Sigma 7.65}(Bi_{8.01}Sb_{0.08})_{\Sigma 8.09}Te_{0.00}S_{20.00}$		$(Cu_{0.16}Ag_{0.18})_{\Sigma 0.34}Pb_{7.82}Bi_8S_{20}$
17)	$(Cu_{0.28}Ag_{0.28})_{\Sigma 0.56}(Fe_{0.08}Pb_{7.32}Cd_{0.12})_{\Sigma 7.52}(Bi_{8.10}Sb_{0.04})_{\Sigma 8.14}Te_{0.00}S_{20.00}$		$(Cu_{0.28}Ag_{0.14})_{\Sigma 0.42}Pb_{7.78}Bi_8S_{20}$
18)	$(Cu_{0.16}Ag_{0.45})_{\Sigma 0.61}(Fe_{0.05}Pb_{7.30}Cd_{0.00})_{\Sigma 7.35}(Bi_{8.19}Sb_{0.00})_{\Sigma 8.19}Te_{0.00}S_{20.00}$		$(Cu_{0.16}Ag_{0.26})_{\Sigma 0.42}Pb_{7.73}Bi_8S_{20}$
19)	$(Cu_{0.17}Ag_{0.53})_{\Sigma 0.70}(Fe_{0.06}Pb_{7.05}Cd_{0.19})_{\Sigma 7.28}(Bi_{8.22}Sb_{0.04}Te_{0.00})_{\Sigma 8.26}S_{20.00}$		$(Cu_{0.17}Ag_{0.27})_{\Sigma 0.44}Pb_{7.79}Bi_8S_{20}$
20)	$(Cu_{0.31}Ag_{0.57})_{\Sigma 0.88}(Fe_{0.05}Pb_{6.95}Cd_{0.11})_{\Sigma 7.12}(Bi_{8.25}Sb_{0.06})_{\Sigma 8.31}Te_{0.00}S_{20.00}$		$(Cu_{0.31}Ag_{0.26})_{\Sigma 0.57}Pb_{7.74}Bi_8S_{20}$
21)	$(Cu_{0.70}Ag_{0.46})_{\Sigma 1.16}(Fe_{0.00}Pb_{6.88}Cd_{0.21})_{\Sigma 7.09}(Bi_{8.16}Sb_{0.04})_{\Sigma 8.20}Te_{0.07}S_{19.93}$		$(Cu_{0.70}Ag_{0.26})_{\Sigma 0.96}Pb_{7.49}Bi_8S_{20}$
22)	$(Cu_{0.67}Ag_{0.56})_{\Sigma 1.23}(Fe_{0.00}Pb_{7.15}Cd_{0.00})_{\Sigma 7.15}(Bi_{8.11}Sb_{0.07})_{\Sigma 8.18}Te_{0.00}S_{20.00}$		$(Cu_{0.67}Ag_{0.38})_{\Sigma 1.05}Pb_{7.51}Bi_8S_{20}$
23)	$(Cu_{0.92}Ag_{0.47})_{\Sigma 1.39}(Fe_{0.00}Pb_{6.87}Cd_{0.24})_{\Sigma 7.11}(Bi_{8.14}Sb_{0.03})_{\Sigma 8.17}Te_{0.05}S_{19.95}$		$(Cu_{0.92}Ag_{0.30})_{\Sigma 1.22}Pb_{7.45}Bi_8S_{20}$
24)	$(Cu_{1.39}Ag_{0.45})_{\Sigma 1.84}(Fe_{0.00}Pb_{6.87}Cd_{0.20})_{\Sigma 7.07}(Bi_{8.01}Sb_{0.04})_{\Sigma 8.05}Te_{0.04}S_{19.96}$		$(Cu_{1.39}Ag_{0.40})_{\Sigma 1.79}Pb_{7.17}Bi_8S_{20}$
25)	$(Cu_{2.48}Ag_{0.33})_{\Sigma 2.81}(Fe_{0.00}Pb_{6.92}Cd_{0.06})_{\Sigma 6.98}(Bi_{7.75}Sb_{0.04})_{\Sigma 7.79}Te_{0.04}S_{19.96}$		$(Cu_{2.48}Ag_{0.33})_{\Sigma 2.81}Pb_{6.98}Bi_{7.79}S_{20}$
26)	$(Cu_{2.85}Ag_{0.33})_{\Sigma 3.18}(Fe_{0.00}Pb_{6.87}Cd_{0.00})_{\Sigma 6.95}(Bi_{7.58}Sb_{0.00})_{\Sigma 7.58}Te_{0.03}S_{19.97}$		$(Cu_{2.85}Ag_{0.33})_{\Sigma 3.18}Pb_{6.95}Bi_{7.62}S_{20}$
27)	$(Cu_{3.30}Ag_{0.32})_{\Sigma 3.62}(Fe_{0.00}Pb_{6.77}Cd_{0.00})_{\Sigma 6.77}(Bi_{7.52}Sb_{0.04})_{\Sigma 7.56}Te_{0.03}S_{19.97}$		$(Cu_{3.30}Ag_{0.32})_{\Sigma 3.62}Pb_{6.77}Bi_{7.56}S_{20}$

The compositions are expressed in wt.%. NA: number of analyses. Standard deviation in terms of the last digit is shown in parentheses. *ch* and *ev* express the absolute and relative error in the charge balance based on the sum of cation and anion charges. $Me^{XS} = Me^{excess}$, represents "interstitial metal", *i.e.*, surplus above 16 Me *apfu* ($Pb_8Bi_8S_{20}$). Pb^* and $(Cu+Ag^*)$ are explained in text. Id_1 is an identification label used in Figures 1a and 1b, and Id_2 is an identification label used in Figures 1c, 2, 4 and 5. Samples: 1: Argentina 1, 2: Argentina 2, 3: Argentina 3, 4: Argentina 4, 5: Tauern Window 1, 6: Tauern Window 2, 7: Tauern Window 3, 8: Tauern Window 4, 9: Tauern Window 5, 10: Tauern Window 6, 11: Tauern Window 7, 12: Tauern Window 8, 13: Tauern Window 9, 14: Felbertal 1, 15: Felbertal 2, 16: Felbertal 3, 17: Felbertal 4, 18: Felbertal 5, 19: Felbertal 6, 20: Felbertal 7, 21: Felbertal 8, 22: Felbertal 9, 23: Felbertal 10, 24: Felbertal 11, 25: Felbertal 12, 26: Felbertal 13, 27: Felbertal 14. Occurrences: 1, 3: Mina La Buena Esperanza, Cerro Aspero; 2, 4: Julio Verne, Salta; 5: Bärenbad, Hollersbachtal; 6, 8, 9, 10, 12, 13: Radhausberg, Gasteinertal; 7, 11: Goldzeche, Raurisertal; 14, 17, 20: K1 orebody; 15, 16, 22, 23-27: K3 orebody; 18: K4 orebody; 19, 21: K7 orebody. The samples are listed in order of the increasing value of (Cu + Ag*) in each of the four groups of analyses (g1–g4). The empirical formulae were calculated on the basis of Te + S = 20 *apfu*. In the formulae, Bi^{excess} is shown in bold; no. 4, 25, 26 and 27 remain unaffected by the $Ag_s + Bi^{excess} \rightarrow 2Pb$ mechanism of substitution.

TABLE 2. AVERAGE RESULTS OF ELECTRON-MICROPROBE ANALYSES OF COSALITE FROM SIX OCCURRENCES, USED FOR SINGLE-CRYSTAL STRUCTURAL INVESTIGATIONS

No.	NA	Cu	Ag	Fe	Pb	Cd	Bi	Sb	Se	Te	S	Total	*ch*	*ev*	Pb*	CuAg*	Me^{XS}
1	20	0.20(2)	0.72(5)	0.13(3)	39.60(15)	0.23(5)	43.38(17)	0.28(12)	0.08(1)	-	16.47(6)	101.09(22)	0.13	0.12	7.92	0.22	0.13
2	21	0.58(6)	0.15(4)	0.03(1)	40.71(35)	0.22(3)	42.76(14)	-	0.07(2)	-	16.33(6)	100.85(34)	0.21	0.19	7.84	0.40	0.23
3a	9	0.64(2)	2.43(6)	0.05(1)	35.67(15)	0.09(3)	42.4(3)	2.37(4)	0.46(4)	-	16.61(8)	100.72(42)	0.05	0.04	7.62	0.75	0.37
3b	8	0.56(2)	3.01(7)	0.05(1)	35.43(19)	0.14(4)	41.24(26)	3.40(6)	0.44(5)	-	16.74(3)	101.02(33)	0.36	0.33	7.64	0.86	0.49
4	19	1.86(10)	0.35(11)	-	38.81(29)	0.32(5)	42.87(18)	0.05(3)	0.07(3)	-	16.51(4)	100.82(28)	-0.21	-0.19	7.38	1.26	0.61
5	28	1.50(10)	1.27(12)	-	37.52(20)	0.14(3)	43.07(29)	0.30(15)	0.11(2)	0.11(3)	16.36(7)	100.37(26)	0.11	0.10	7.40	1.24	0.64
6	29	1.58(3)	3.07(15)	0.05(3)	35.95(32)	0.19(5)	43.20(22)	-	0.11(2)	0.08(1)	16.39(5)	100.62(5)	-0.01	-0.01	6.99	2.02	1.01

1) $(Cu_{0.12}Ag_{0.26})_{\Sigma 0.38}(Fe_{0.09}Pb_{7.43}Cd_{0.08})_{\Sigma 7.60}(Bi_{8.07}Sb_{0.09})_{\Sigma 8.16}Te_{0.00}Se_{0.04}S_{19.96}$, or, after $Ag_s + Bi^{excess} \rightarrow 2Pb$, $(Cu_{0.12}Ag_{0.10})_{\Sigma 0.22}Pb_{7.92}Bi_8S_{20}$
2) $(Cu_{0.36}Ag_{0.06})_{\Sigma 0.42}(Fe_{0.02}Pb_{7.70}Cd_{0.08})_{\Sigma 7.80}(Bi_{8.02}Sb_{0.00})_{\Sigma 8.02}Te_{0.00}Se_{0.03}S_{19.97}$ $(Cu_{0.36}Ag_{0.04})_{\Sigma 0.40}Pb_{7.84}Bi_8S_{20}$
3a) $(Cu_{0.38}Ag_{0.86})_{\Sigma 1.24}(Fe_{0.03}Pb_{6.57}Cd_{0.03})_{\Sigma 6.63}(Bi_{7.75}Sb_{0.74})_{\Sigma 8.49}Te_{0.00}Se_{0.22}S_{19.78}$ $(Cu_{0.38}Ag_{0.37})_{\Sigma 0.75}Pb_{7.62}Bi_8S_{20}$
3b) $(Cu_{0.34}Ag_{1.06})_{\Sigma 1.40}(Fe_{0.03}Pb_{6.48}Cd_{0.05})_{\Sigma 6.56}(Bi_{7.48}Sb_{1.06})_{\Sigma 8.54}Te_{0.00}Se_{0.21}S_{19.79}$ $(Cu_{0.34}Ag_{0.52})_{\Sigma 0.86}Pb_{7.64}Bi_8S_{20}$
4) $(Cu_{1.14}Ag_{0.12})_{\Sigma 1.26}(Fe_{0.00}Pb_{7.27}Cd_{0.11})_{\Sigma 7.38}(Bi_{7.96}Sb_{0.02})_{\Sigma 7.97}Te_{0.00}Se_{0.03}S_{19.97}$ $(Cu_{1.14}Ag_{0.12})_{\Sigma 1.26}Pb_{7.30}Bi_{7.97}S_{20}$
5) $(Cu_{0.92}Ag_{0.46})_{\Sigma 1.38}(Fe_{0.00}Pb_{7.07}Cd_{0.05})_{\Sigma 7.12}(Bi_{8.04}Sb_{0.10})_{\Sigma 8.14}Te_{0.03}Se_{0.05}S_{19.91}$ $(Cu_{0.92}Ag_{0.32})_{\Sigma 1.24}Pb_{7.40}Bi_8S_{20}$
6) $(Cu_{0.97}Ag_{1.11})_{\Sigma 2.08}(Fe_{0.04}Pb_{6.77}Cd_{0.07})_{\Sigma 6.87}(Bi_{8.06}Sb_{0.00})_{\Sigma 8.06}Te_{0.02}Se_{0.05}S_{19.93}$ $(Cu_{0.97}Ag_{1.05})_{\Sigma 2.02}Pb_{6.99}Bi_8S_{20}$

Samples listed: 1: Felbertal, K1 orebody, Felbertal, Pinzgau; 2: Habachtal, Pinzgau; 3a: Altenberg 1, Lungau; 3b: Altenberg 2, Lungau; 4: Ocna de Fier, Romania; 5 Erzwiess, Gasteinertal; 6: Schareck, Schareck-Siglitz, Gasteinertal. Sample 3a (Altenberg 1) was studied structurally. Samples are ordered according to the increasing Cu + Ag* value. Me^{XS}: Me^{excess}. The symbols used are as defined in Table 1.

TABLE 3. GENERAL INFORMATION ABOUT THE COLLECTION OF SINGLE-CRYSTAL X-RAY DATA AND THE STRUCTURE REFINEMENTS OF COSALITE

Diffractometer	Bruker AXS CCD system
X-ray radiation source	fine-focus sealed tube, Mo*Kα*
X-ray radiation monochromator	graphite
X-ray power	50 kV, 30 mA
Temperature	298 K
Rotation width	0.3°
Frame size (in pixels)	512 * 512 pixels
Resolution (Å)	0.75
Crystal form	irregular
Crystal color	metallic
Crystal system	orthorhombic
Space group	*Pnma*
Z	2
Absorption method	empirical
Refinement	on F_o^2
Source of atomic scattering factors	*International Tables for Crystallography* (1992, Vol. C, Tables 4.2.6.8 and 6.1.1.4)
Structure solution	*SHELXS97* (Sheldrick 1997a)
Structure refinement	*SHELXL97* (Sheldrick 1997b)
$R_{INT} = \Sigma \lvert F_o^2 - F_c^2(\text{mean})\rvert / \Sigma F_o^2$	Goof = $\{(\Sigma w[F_o^2 - F_c^2] / [n\text{-}p])\}^{1/2}$
$R_\sigma = \Sigma \sigma(F_o^2) / \Sigma F_o^2$	$w = 1 / (\sigma^2[F_o^2] + [0.2 * P]^2)$
$R_1 = \Sigma \lVert F_o\rvert - \lvert F_c\rVert / \Sigma \lvert F_o\rvert$	$P = (\max(F_o^2, 0) + 2 F_c^2) / 3$
$wR_2 = \{(\Sigma w[F_o^2 - F_c^2]^2 / \Sigma w[F_o^2]^2)\}^{1/2}$	

on the sulfosalt associations at the Felbertal deposit can be found in Topa (2001), Topa *et al.* (2001), and Topa *et al.* (2003b).

Selected compositions of cosalite taken from literature, considered to be of good quality, are summarized in Figure 1d. With the exception of a presumed cosalite–galena intergrowth after heyrovskýite from Moaralm (Paar *et al.* 1980), all these cosalite compositions (Fig. 1d) follow closely the trend found in our analyses (Fig. 1c).

As a consequence of the monovalent character of the metals (Cu and Ag) substituting for Pb, as inferred already by Karup-Møller (1977) and confirmed by our data, the amount of cations in *pfu* is not constant. Therefore, the formulae used in this contribution are based on 20 sulfur *apfu* (*i.e.*, contents of two asymmetric units or one half of the unit cell of cosalite, idealized for large cations as the $Pb_8Bi_8S_{20}$ formula, giving Z = 2, Tables 1, 2). The reliability of the analytical data can be evaluated from the absolute (*ch*) and relative (*ev*) error in charge balance based on the sum of cation and anion charges, calculated with normalized atomic % data (Moëlo *et al.* 1987). Analyses with the values of *ch* outside the range [–2, 2] were discarded. The scatter of regression trends in the subsequent composition diagrams (Figs. 2a–g) is primarily due to the scatter of analytical estimates of sulfur contents. In order to eliminate the influence of instrumental differences on the derivations, only the presently obtained data, on the same electron-microprobe apparatus, under the same conditions and employing the same set of standards, will be used (*i.e.*, no literature data are used).

The balance of large cations in an "ideal" (non-existent) cosalite [*i.e.*, the model used by Weitz & Hellner (1960), with four independent sites of Bi, four independent sites of Pb, and ten independent sites of S] gives the formula $Pb_8Bi_8S_{20}$, Z = 2. In the empirical formulae obtained from our analyses, based on 20 S *apfu*, the contents of Bi (+ antimony) vary between 7.98

TABLE 4. CRYSTAL DATA AND RESULTS OF THE STRUCTURE REFINEMENTS FOR COSALITE

	1. Felbertal	2. Habachtal	3. Altenberg 1	4. Ocna de Fier	5. Erzwiess	6. Schareck
Formula	$Cu_{0.12}Ag_{0.26}$ $Pb_{7.60}Bi_{8.16}S_{20}$	$Cu_{0.36}Ag_{0.06}$ $Pb_{7.80}Bi_{8.02}S_{20}$	$Cu_{0.38}Ag_{0.86}$ $Pb_{6.63}Bi_{8.49}S_{20}$	$Cu_{1.14}Ag_{0.12}$ $Pb_{7.38}Bi_{7.97}S_{20}$	$Cu_{0.92}Ag_{0.46}$ $Pb_{7.12}Bi_{8.14}S_{20}$	$Cu_{0.96}Ag_{1.11}$ $Pb_{6.87}Bi_{8.06}S_{20}$
Formula weight	3977.51	3962.65	3828.54	3921.21	3910.94	3930.34
a (Å)	23.870(4)	23.894(5)	23.652(1)	23.816(2)	23.846(4)	23.879(2)
b (Å)	4.0647(6)	4.0616(9)	4.0539(3)	4.0408(3)	4.0559(8)	4.0453(5)
c (Å)	19.130(3)	19.143(4)	19.095(1)	19.057(1)	19.066(4)	19.017(7)
V (Å^3)	1856.1(5)	1857.8(7)	1830.8(2)	1833.9(2)	1844.0(6)	1837.0(3)
D_x (Mg m^{-3})	7.117	7.084	6.945	7.106	7.169	7.116
Crystal size (mm)	0.12 × 0.09 × 0.05	0.12 × 0.05 × 0.03	0.12 × 0.06 × 0.04	0.10 × 0.07 × 0.04	0.15 × 0.09 × 0.06	0.06 × 0.04 × 0.02
μ (mm^{-1})	74.62	74.38	68.49	73.66	74.38	72.16
Time per frame (s)	30	40	30	30	15	90
Total # of frames	1940	3400	2485	2485	3400	2485
T_{min}, T_{max}	0.0567, 0.2881	0.0373, 0.1761	0.0171, 0.0757	0.0007, 0.0139	0.1478, 0.6028	0.1478, 0.6028
Maximum 2θ(°)	53.34	56.84	61.06	61.11	56.60	61.11
Measured reflections	11003	15973	25683	25825	26129	24493
Index range	$-29 \le h \le 29$ $-5 \le k \le 4$ $-21 \le l \le 22$	$-31 \le h \le 27$ $-5 \le k \le 5$ $-25 \le l \le 24$	$-33 \le h \le 33$ $-3 \le k \le 5$ $-27 \le l \le 27$	$-34 \le h \le 34$ $-5 \le k \le 4$ $-27 \le l \le 26$	$-31 \le h \le 31$ $-5 \le k \le 5$ $-25 \le l \le 25$	$-34 \le h \le 34$ $-5 \le k \le 4$ $-26 \le l \le 27$
Unique reflections	2065	2537	3034	3097	2574	3102
Reflections > 2σ(*I*)	1598	1785	2262	2097	2229	2130
R_{INT} (%)	7.83	17.99	11.40	13.97	12.45	12.45
R_o (%)	4.60	9.45	5.23	6.79	6.64	6.64
Number of least-. squares parameters	126	125	128	125	128	126
GooF	1.007	0.889	1.032	0.898	1.038	0.898
R_1, $F_o > 4\,\sigma(F_o)$ (%)	3.62	5.31	4.30	6.63	2.80	4.74
R_1, all data (%)	4.85	8.28	6.33	9.32	3.40	7.77
wR_2 (on F_o^2) (%)	9.33	11.47	10.80	16.55	6.62	10.95
Final diff. Fourier map (Å^{-3})	−1.747 to +2.146	−2.640 to +6.698	−3.65 to +4.71	−2.917 to +5.600	−2.056 to +3.363	−4.196 to +4.385

and 8.51 *apfu*, with the exception of the copper-rich substitutional rims in cosalite from Felbertal, where they can drop as low as 7.56 *apfu*. Lead (+ cadmium + iron) varies between 6.35 and 7.84 *apfu*, Cu between 0.12 and 1.45 *apfu*, with the exception of the copper-rich substitutional rims in cosalite from Felbertal, where they can reach 3.3 *apfu*, whereas Ag varies between 0.06 and 1.18 *apfu* (Tables 1, 2). The sum of cations in the triangular diagrams (Fig. 1) is constrained to 100, *i.e.*, the effects of variations in Pb/Bi in them combine with those of cation excess above 16 *apfu*, displacing the points on the principal compositional line (subhorizontal in Figs. 1b, 1c) away from the Bi vertex.

Plotting individual compositions in the correlation diagrams based on the formula with 20 S *apfu* reveals, first of all, that Cu and Ag can be considered uncorrelated, with Cu at two or even three distinct levels of concentration (Fig. 2a). The (Cu + Ag) *versus* Pb and (Cu + Ag) *versus* Bi plots (Figs. 2b and 2c) are practically antithetic: in "normal" cosalite (the bulk of the samples), 2(Cu + Ag) enters at the expense of Pb (Fig. 2b), whereas the contents of Bi remain broadly constant (Fig. 2c). Only the silver-rich material from Altenberg lies outside the main body of data, revealing that its combined high contents of Ag and Bi occur at the additional expense of Pb (compare Figs. 2a, b and c). The anomalous, Cu-rich replacement rims from Felbertal show that the "excess" (Cu + Ag) portion in them is incorporated primarily at the expense of bismuth (Figs. 2b, 2c). Back-scattered electron photographs and the elemental X-ray maps (Fig. 3) show extreme enrichment in Cu, without distinct boundaries, and connected with depletion in Cd and slight depletion in Ag and Bi within the first ~20 μm along the fissures that are filled by native bismuth or bismuthinite (or both), galena and other, unresolved phases rich in Cd and Ag.

The combination of the above mechanisms results in a nearly linear replacement trend of 2(Cu + Ag) for 1(Pb + Bi) *apfu* (Fig. 2d). The same trend loses its scatter if atomic % are used instead of atoms *pfu*, underlining the importance of the errors introduced by variation in the S values (not illustrated, but deposited). The presence of excess Bi, above 8 *apfu*, especially in the sample 3 (Altenberg 3a) is explained by the Ag + Bi ↔ 2 Pb substitution in at least one of the Pb sites. As explained later, this was confirmed by the structure

TABLE 5. COORDINATES, SITE OCCUPANCY, EQUIVALENT AND ANISOTROPIC DISPLACEMENT PARAMETERS OF ATOMS IN COSALITE FROM SIX LOCALITIES

ATOM	*x*	*y*	*z*	*sof*	U_{eq}	U_{11}	U_{22}	U_{33}	U_{13}
				1 Felbertal					
Bi1	0.15479(3)	0.75	0.98271(4)		0.0366(2)	0.0368(4)	0.0390(5)	0.0339(5)	-0.0009(3)
Bi2	0.30228(3)	0.75	0.09385(5)		0.0391(2)	0.0382(4)	0.0418(5)	0.0371(5)	-0.0001(3)
*Me*3	0.01046(3)	0.25	0.09059(5)		0.0404(2)	0.0405(5)	0.0407(5)	0.0399(5)	-0.0013(4)
Bi4	0.17144(3)	0.25	0.18658(4)		0.0381(2)	0.0387(4)	0.0405(5)	0.0352(5)	0.0009(3)
*Me*1	0.04032(4)	0.75	0.27444(5)	0.986(5)	0.0417(4)	0.0407(5)	0.0430(6)	0.0414(6)	0.0002(4)
Ag1	0.04032(4)	0.75	0.27444(5)	0.014(5)	0.0417(4)	0.0407(5)	0.0430(6)	0.0414(6)	0.0002(4)
*Me*2	0.43393(4)	0.25	0.03475(6)	0.918(3)	0.0447(4)	0.0415(6)	0.0458(6)	0.0467(9)	-0.0018(5)
Pb3	0.20582(4)	0.75	0.38343(5)		0.0477(3)	0.0476(5)	0.0452(5)	0.0504(6)	0.0005(4)
Pb4	0.37334(4)	0.75	0.29318(5)		0.0471(3)	0.0507(5)	0.0482(5)	0.0424(5)	0.0007(4)
Cu1	0.419(3)	0.25	0.978(3)	0.057(13)	0.05(2)	0.08(4)	0.04(3)	0.04(4)	0.02(3)
Cu2	0.452(2)	0.25	0.110(4)	0.075(17)	0.09(3)	0.05(3)	0.07(4)	0.16(8)	0.03(4)
S1	0.1389(2)	0.25	0.4776(3)		0.041(1)	0.042(3)	0.043(3)	0.037(3)	-0.001(2)
S2	0.2293(2)	0.25	0.0296(3)		0.039(1)	0.037(3)	0.039(3)	0.042(3)	-0.005(2)
S3	0.9983(3)	0.75	0.4140(3)		0.046(1)	0.048(3)	0.045(3)	0.045(4)	0.004(3)
S4	0.3636(2)	0.25	0.1524(3)		0.040(1)	0.040(3)	0.044(3)	0.036(3)	-0.003(2)
S5	0.4642(2)	0.25	0.2819(3)		0.039(1)	0.038(3)	0.037(3)	0.041(3)	-0.005(2)
S6	0.2380(2)	0.75	0.2287(3)		0.036(1)	0.035(3)	0.034(3)	0.038(3)	-0.001(2)
S7	0.0877(2)	0.75	0.1295(3)		0.039(1)	0.040(3)	0.038(3)	0.039(3)	-0.001(2)
S8	0.1247(2)	0.25	0.3075(3)		0.037(1)	0.038(3)	0.040(3)	0.033(3)	0.002(2)
S9	0.2956(2)	0.25	0.3616(3)		0.037(1)	0.034(2)	0.041(3)	0.035(3)	-0.001(2)
S10	0.4165(2)	0.75	0.4343(3)		0.040(1)	0.037(3)	0.043(3)	0.041(3)	-0.001(2)
				2 Habachtal					
Bi1	0.15501(4)	0.75	0.98209(5)		0.0185(2)	0.0153(5)	0.0159(5)	0.0242(5)	-0.0003(4)
Bi2	0.30262(4)	0.75	0.09318(5)		0.0190(2)	0.0138(5)	0.0175(4)	0.0257(5)	-0.0002(4)
*Me*3	0.01051(4)	0.25	0.08977(5)		0.0214(3)	0.0173(5)	0.0184(5)	0.0285(6)	-0.0014(4)
Bi4	0.17134(4)	0.25	0.18559(5)		0.0191(2)	0.0168(5)	0.0173(5)	0.0231(5)	0.0004(4)
*Me*1	0.04038(4)	0.75	0.27356(5)		0.0226(3)	0.0193(6)	0.0188(5)	0.0296(6)	0.0008(4)
*Me*2	0.43418(5)	0.25	0.03430(3)	0.867(7)	0.0234(6)	0.0164(7)	0.0206(6)	0.0330(9)	-0.0005(6)
Pb3	0.20592(5)	0.75	0.38200(6)		0.0290(3)	0.0237(6)	0.0221(5)	0.0412(7)	0.0001(5)
Pb4	0.37356(6)	0.75	0.29288(6)		0.0288(3)	0.0295(6)	0.0245(5)	0.0324(6)	0.0010(5)
Cu1	0.423(2)	0.25	0.978(3)	0.13(2)	0.07(3)	0.07(4)	0.02(2)	0.11(5)	0.09(4)
Cu2	0.447(1)	0.25	0.104(3)	0.13(2)	0.07(2)	0.02(2)	0.03(2)	0.15(6)	0.07(3)
S1	0.1385(3)	0.25	0.4764(3)		0.023(1)	0.022(4)	0.025(3)	0.021(3)	-0.003(3)
S2	0.2297(3)	0.25	0.0296(4)		0.021(1)	0.015(3)	0.019(3)	0.029(3)	-0.003(3)
S3	0.9996(3)	0.75	0.4135(4)		0.027(1)	0.020(4)	0.029(3)	0.031(4)	0.004(3)
S4	0.3635(3)	0.25	0.1524(3)		0.021(1)	0.018(3)	0.021(3)	0.025(3)	-0.004(3)
S5	0.4640(3)	0.25	0.2828(3)		0.021(1)	0.020(3)	0.019(3)	0.024(3)	-0.002(3)
S6	0.2382(3)	0.75	0.2280(3)		0.020(1)	0.017(3)	0.016(3)	0.025(3)	-0.001(3)
S7	0.0884(3)	0.75	0.1286(4)		0.022(1)	0.020(3)	0.015(3)	0.032(4)	-0.002(3)
S8	0.1251(3)	0.25	0.3070(3)		0.020(1)	0.019(3)	0.019(3)	0.023(3)	0.004(3)
S9	0.2961(3)	0.25	0.3609(3)		0.018(1)	0.018(3)	0.012(3)	0.023(3)	-0.002(3)
S10	0.4156(3)	0.75	0.4338(3)		0.019(1)	0.0120(3)	0.014(3)	0.030(3)	0.001(3)
				3 Altenberg 1					
Bi1	0.15300(2)	0.75	0.98546(3)		0.0246(2)	0.0259(3)	0.0289(5)	0.0192(3)	-0.0010(2)
Bi2	0.30155(3)	0.75	0.09556(4)	0.72(1)	0.0240(3)	0.0236(4)	0.0284(5)	0.0201(4)	-0.0002(2)
Sb2	0.30155(3)	0.75	0.09556(4)	0.28(1)	0.0240(3)	0.0236(4)	0.0285(5)	0.0201(4)	-0.0002(2)
*Me*3	0.01034(3)	0.25	0.09519(4)		0.0281(2)	0.0294(3)	0.0297(5)	0.0252(3)	-0.0016(2)
Bi4	0.17259(3)	0.25	0.18970(4)	0.833(10)	0.0237(3)	0.0253(4)	0.0271(5)	0.0189(4)	0.0005(2)
Sb4	0.17259(3)	0.25	0.18970(4)	0.167(10)	0.0237(3)	0.0253(4)	0.0271(5)	0.0189(4)	0.0005(2)
*Me*1	0.04200(3)	0.75	0.27776(4)	0.808(9)	0.0287(5)	0.0286(4)	0.0330(6)	0.0244(5)	0.0011(3)
Ag1	0.04200(3)	0.75	0.27776(4)	0.192(9)	0.0287(5)	0.027(1)	0.0331(6)	0.0244(5)	0.0011(3)
*Me*2	0.43385(3)	0.25	0.03752(5)	0.834(5)	0.0330(3)	0.0315(5)	0.0356(7)	0.0318(5)	-0.0035(3)
Pb3	0.20675(3)	0.75	0.38825(4)		0.0350(2)	0.0366(4)	0.0318(5)	0.0366(4)	-0.0014(3)
Pb4	0.37231(3)	0.75	0.29367(4)		0.0346(2)	0.0413(4)	0.0345(5)	0.0279(4)	0.0010(3)
Ag2	0.4200(5)	0.25	0.9739(7)	0.139(8)	0.043(5)	0.042(7)	0.039(9)	0.047(8)	0.017(5)
Cu2	0.4510(7)	0.25	0.115(1)	0.203(16)	0.064(8)	0.053(9)	0.05(1)	0.09(2)	-0.007(8)
S1	0.1411(2)	0.25	0.4799(2)		0.0267(9)	0.032(2)	0.031(3)	0.017(2)	0.003(1)
S2	0.2272(2)	0.25	0.0304(2)		0.0261(9)	0.026(2)	0.032(3)	0.021(2)	-0.003(1)
S3	0.9993(2)	0.75	0.4110(3)		0.034(1)	0.034(2)	0.035(3)	0.032(2)	0.007(2)
S4	0.3625(2)	0.25	0.1545(2)		0.031(1)	0.028(2)	0.046(4)	0.017(2)	-0.005(1)
S5	0.4664(2)	0.25	0.2789(2)		0.0236(9)	0.022(2)	0.025(3)	0.024(2)	-0.003(1)
S6	0.2386(2)	0.75	0.2317(2)		0.0261(9)	0.021(2)	0.036(3)	0.021(2)	-0.001(1)
S7	0.0874(2)	0.75	0.1327(2)		0.0276(9)	0.029(2)	0.032(3)	0.021(2)	0.001(2)
S8	0.1239(2)	0.25	0.3098(2)		0.0239(9)	0.029(2)	0.031(3)	0.012(2)	0.001(1)
S9	0.2981(2)	0.25	0.3634(2)		0.0205(8)	0.023(2)	0.023(3)	0.015(2)	-0.001(1)
S10	0.4220(2)	0.75	0.4355(3)		0.030(1)	0.030(2)	0.034(3)	0.025(2)	0.006(2)

TABLE 5 (cont'd). COORDINATES, SITE OCCUPANCY, EQUIVALENT AND ANISOTROPIC DISPLACEMENT PARAMETERS OF ATOMS IN COSALITE FROM SIX LOCALITIES

ATOM	*x*	*y*	*z*	*sof*	U_{eq}	U_{11}	U_{22}	U_{33}	U_{13}
				4 Ocna de Fier					
Bi1	0.15500(4)	0.75	0.98212(4)		0.0335(3)	0.0322(4)	0.0399(6)	0.0284(4)	-0.0006(2)
Bi2	0.30494(4)	0.75	0.09192(5)		0.0352(3)	0.0332(4)	0.0429(6)	0.0295(4)	-0.0006(3)
*Me*3	0.01088(4)	0.25	0.08944(5)		0.0370(3)	0.0360(4)	0.0422(7)	0.0328(5)	-0.0015(3)
Bi4	0.17215(4)	0.25	0.18459(4)		0.0339(3)	0.0330(4)	0.0404(6)	0.0284(4)	0.0004(3)
*Me*1	0.04037(4)	0.75	0.27450(5)		0.0378(3)	0.0354(4)	0.0432(7)	0.0349(5)	0.0007(3)
*Me*2	0.43712(7)	0.25	0.03262(9)	0.695(8)	0.0480(7)	0.0398(9)	0.0540(9)	0.0500(9)	-0.0054(6)
Pb3	0.20576(5)	0.75	0.38268(6)		0.0455(3)	0.0430(5)	0.0470(8)	0.0470(6)	-0.0011(4)
Pb4	0.37236(5)	0.75	0.29199(6)		0.0454(3)	0.0490(6)	0.0499(8)	0.0372(5)	0.0015(4)
Cu1	0.4134(5)	0.25	0.9710(6)	0.34(2)	0.046(4)	0.052(7)	0.035(7)	0.050(7)	0.011(4)
Cu2	0.4512(5)	0.25	0.1115(8)	0.39(3)	0.065(6)	0.047(6)	0.07(1)	0.080(9)	-0.008(5)
S1	0.1371(3)	0.25	0.4761(3)		0.036(1)	0.037(4)	0.045(4)	0.028(3)	-0.004(2)
S2	0.2304(3)	0.25	0.0284(3)		0.035(1)	0.032(3)	0.040(4)	0.033(3)	-0.004(2)
S3	0.9994(3)	0.75	0.4118(4)		0.047(2)	0.046(3)	0.046(5)	0.049(4)	0.012(3)
S4	0.3643(3)	0.25	0.1519(4)		0.039(1)	0.034(3)	0.040(4)	0.043(3)	-0.008(2)
S5	0.4652(3)	0.25	0.2811(3)		0.034(1)	0.031(3)	0.037(4)	0.036(3)	-0.0014(2)
S6	0.2381(3)	0.75	0.2275(3)		0.036(1)	0.032(3)	0.042(4)	0.032(3)	-0.003(2)
S7	0.0888(3)	0.75	0.1273(3)		0.035(1)	0.035(3)	0.031(4)	0.040(3)	0.001(2)
S8	0.1245(3)	0.25	0.3062(3)		0.035(1)	0.033(3)	0.040(4)	0.033(3)	0.001(2)
S9	0.2961(2)	0.25	0.3600(3)		0.032(1)	0.030(2)	0.037(4)	0.028(2)	0.001(2)
S10	0.4162(3)	0.75	0.4330(3)		0.037(1)	0.035(3)	0.045(4)	0.032(3)	0.004(2)
				5 Erzwiess					
Bi1	0.15453(2)	0.75	0.98219(2)		0.0144(1)	0.0117(2)	0.0176(2)	0.0139(2)	-0.0004(2)
Bi2	0.30367(2)	0.75	0.09249(2)		0.0161(1)	0.0130(2)	0.0196(2)	0.0155(2)	-0.0009(2)
*Me*3	0.01079(2)	0.25	0.09038(2)		0.0179(1)	0.0160(2)	0.0196(2)	0.0181(2)	-0.0014(2)
Bi4	0.17164(2)	0.25	0.18539(2)		0.0154(1)	0.0135(2)	0.0185(2)	0.0142(2)	0.0008(2)
*Me*1	0.04031(5)	0.75	0.27519(5)	0.944(5)	0.0195(2)	0.0160(5)	0.0227(3)	0.0199(5)	0.0015(3)
Ag1	0.048(2)	0.75	0.264(5)	0.056(5)	0.0195(2)	0.0160(5)	0.0227(3)	0.0199(5)	0.0015(3)
*Me*2	0.43582(3)	0.25	0.0343(4)	0.699(2)	0.0266(3)	0.0185(4)	0.0285(4)	0.0328(5)	-0.0040(3)
Pb3	0.20579(2)	0.75	0.3833(3)		0.0270(1)	0.0247(3)	0.0248(3)	0.0315(3)	-0.0003(2)
Pb4	0.37240(2)	0.75	0.2921(3)		0.0265(1)	0.0310(3)	0.0268(3)	0.0218(3)	0.0008(2)
Ag2	0.4160(2)	0.25	0.9726(3)	0.252(4)	0.043(2)	0.040(3)	0.040(2)	0.047(3)	0.007(2)
Cu2	0.4503(2)	0.25	0.1141(3)	0.358(7)	0.046(2)	0.029(3)	0.046(2)	0.064(4)	-0.011(3)
S1	0.1383(1)	0.25	0.4765(2)		0.0187(6)	0.019(2)	0.024(2)	0.013(1)	-0.001(1)
S2	0.2292(1)	0.25	0.0292(2)		0.0178(6)	0.016(2)	0.021(2)	0.017(1)	-0.004(1)
S3	0.9988(2)	0.75	0.4099(2)		0.0276(7)	0.023(2)	0.027(2)	0.033(2)	0.005(1)
S4	0.3633(1)	0.25	0.1531(2)		0.0192(6)	0.017(2)	0.024(2)	0.017(1)	-0.007(1)
S5	0.4655(1)	0.25	0.2807(2)		0.0184(6)	0.015(2)	0.021(2)	0.019(2)	-0.003(1)
S6	0.2378(1)	0.75	0.2281(1)		0.0155(5)	0.012(1)	0.019(1)	0.015(1)	-0.001(2)
S7	0.0883(1)	0.75	0.1285(2)		0.0171(6)	0.014(1)	0.021(2)	0.017(1)	-0.002(2)
S8	0.1236(1)	0.25	0.3066(1)		0.0172(2)	0.019(2)	0.022(2)	0.011(1)	0.003(2)
S9	0.2961(1)	0.25	0.3606(1)		0.0147(5)	0.016(1)	0.016(1)	0.012(1)	-0.001(2)
S10	0.4165(2)	0.75	0.4335(2)		0.0168(5)	0.014(1)	0.018(1)	0.018(1)	0.001(2)
				6 Schareck					
Bi1	0.15379(3)	0.75	0.98238(3)		0.0150(2)	0.0161(4)	0.0130(4)	0.0158(3)	-0.0008(2)
Bi2	0.30314(3)	0.75	0.09282(4)		0.0158(2)	0.0159(4)	0.0143(4)	0.0172(3)	-0.0012(2)
*Me*3	0.01100(3)	0.25	0.09054(4)		0.0180(2)	0.0191(4)	0.0145(4)	0.0204(3)	-0.0016(3)
Bi4	0.17111(3)	0.25	0.18588(3)		0.0155(2)	0.0170(4)	0.0138(4)	0.0158(3)	0.0009(3)
*Me*1	0.03981(4)	0.75	0.27589(4)	0.922(10)	0.0201(3)	0.0196(5)	0.0182(5)	0.0226(4)	0.0009(3)
Ag1	0.03981(4)	0.75	0.27589(4)	0.078(10)	0.0201(3)	0.0196(5)	0.0182(5)	0.0226(4)	0.0009(3)
*Me*2	0.43564(7)	0.25	0.03615(8)	0.524(5)	0.0236(6)	0.0161(8)	0.024(1)	0.0304(9)	-0.0016(6)
Pb3	0.20572(4)	0.75	0.38512(5)		0.0281(2)	0.0284(5)	0.0209(5)	0.0351(4)	-0.0005(3)
Pb4	0.37095(4)	0.75	0.29190(4)		0.0276(2)	0.0363(5)	0.0222(5)	0.0243(4)	0.0014(3)
Ag2	0.4218(2)	0.25	0.9757(3)	0.432(10)	0.042(2)	0.033(3)	0.035(3)	0.058(3)	0.012(2)
Cu2	0.4499(3)	0.25	0.1195(4)	0.463(10)	0.037(3)	0.023(4)	0.039(5)	0.050(5)	0.001(3)
S1	0.1392(2)	0.25	0.4775(2)		0.021(1)	0.024(3)	0.023(3)	0.015(2)	-0.004(2)
S2	0.2285(3)	0.25	0.0296(3)		0.019(1)	0.019(3)	0.013(3)	0.025(2)	-0.004(2)
S3	0.9962(3)	0.75	0.4078(3)		0.034(4)	0.027(3)	0.038(4)	0.036(3)	0.008(2)
S4	0.3615(2)	0.25	0.1542(3)		0.020(1)	0.020(3)	0.022(3)	0.018(2)	-0.009(2)
S5	0.4665(2)	0.25	0.2790(3)		0.020(1)	0.014(2)	0.020(3)	0.025(2)	-0.003(2)
S6	0.2371(2)	0.75	0.2285(2)		0.016(1)	0.017(2)	0.017(3)	0.014(2)	-0.002(2)
S7	0.0887(2)	0.75	0.1281(2)		0.017(1)	0.019(3)	0.014(3)	0.019(2)	-0.001(2)
S8	0.1221(2)	0.25	0.3071(2)		0.016(1)	0.019(2)	0.015(3)	0.014(2)	-0.001(2)
S9	0.2965(2)	0.25	0.3604(2)		0.015(1)	0.018(2)	0.009(2)	0.019(2)	-0.005(2)
S10	0.4168(2)	0.75	0.4331(2)		0.017(1)	0.018(2)	0.015(3)	0.019(2)	0.004(2)

TABLE 6. SELECTED CATION–ANION DISTANCES (Å) IN COSALITE

1 Felbertal

Bi1	Bi2	*Me*3	Bi4	*Me*1	*Me*2	Pb3	Pb4	Cu1	Cu2
S9 2.602(6)	S1 2.630(6)	S5 2.678(6)	S8 2.568(6)	S3 2.852(6)	S3 2.730(5) ×2	S9 2.983(4) ×2	S10 2.890(4)	S3 2.343(68)	S4 2.261(53)
S10 2.808(4) ×2	S4 2.744(4) ×2	S7 2.843(4) ×2	S6 2.701(3) ×2	S8 2.930(4) ×2	S4 2.808(6)	S6 3.059(6)	S5 2.980(4) ×2	S1 2.444(40) ×2	S3 2.359(27) ×2
S2 2.846(4) ×2	S2 2.945(4) ×2	S10 3.064(4) ×2	S7 3.053(4) ×2	S5 2.932(4) ×2	S3 2.820(6)	S1 3.151(4) ×2	S9 3.047(4) ×2	S3 3.475(52) ×2	S5 3.301(77)
S7 3.233(6)	S6 3.001(6)	S10 3.461(6)	S2 3.305(6)	S7 2.995(6)	S1 2.889(4) ×2	S8 3.161(4) ×2	S4 3.382(5) ×2	S4 3.580(60)	
						S2 3.196(6)	S6 3.461(5)		

2 Habachtal

Bi1	Bi2	*Me*3	Bi4	*Me*1	*Me*2	Pb3	Pb4	Cu1	Cu2
S9 2.597(6)	S1 2.641(6)	S5 2.681(6)	S8 2.573(6)	S3 2.849(8)	S3 2.751(5) ×2	S9 2.988(5) ×2	S10 2.879(6)	S3 2.225(51)	S4 2.195(39)
S10 2.797(5) ×2	S4 2.743(5) ×2	S7 2.852(5) ×2	S6 2.708(5) ×2	S5 2.936(5) ×2	S3 2.804(8)	S6 3.047(6)	S5 2.972(5) ×2	S1 2.507(28) ×2	S3 2.414(20) ×2
S2 2.852(5) ×2	S2 2.940(5) ×2	S10 3.077(5) ×2	S7 3.042(5) ×2	S8 2.938(5) ×2	S4 2.822(7)	S8 3.149(5) ×2	S9 3.041(5) ×2	S3 3.435(44) ×2	S5 3.447(57)
S7 3.226(8)	S6 3.005(6)	S10 3.469(6)	S2 3.296(6)	S7 3.002(8)	S1 2.893(5)	S1 3.160(5) ×2	S4 3.378(5) ×2	S4 3.560(50)	
						S2 3.217(6)	S6 3.465(7)		

3 Altenberg 1

Bi1	Bi2	*Me*3	Bi4	*Me*1	*Me*2	Pb3	Pb4	Ag2	Cu2
S9 2.602(4)	S1 2.592(4)	S5 2.620(4)	S8 2.566(4)	S3 2.737(8)	S3 2.733(3) ×2	S9 3.000(3) ×2	S10 2.952(4)	S3 2.255(13)	S4 2.223(18)
S2 2.815(3) ×2	S4 2.730(3) ×2	S7 2.818(3) ×2	S6 2.682(3) ×2	S8 2.869(4) ×2	S4 2.799(4)	S6 3.083(4)	S9 2.994(3) ×2	S1 2.492(7) ×2	S3 2.380(10) ×2
S10 2.857(3) ×2	S2 2.958(3) ×2	S10 2.970(3) ×2	S7 3.059(3) ×2	S5 2.912(4) ×2	S3 2.887(6)	S1 3.096(3) ×2	S5 3.023(3) ×2	S3 3.529(11) ×2	S5 3.147(23)
S7 3.209(4)	S6 2.995(4)	S10 3.444(4)	S2 3.305(4)	S7 2.973(7)	S1 2.909(3) ×2	S2 3.132(4)	S4 3.350(3) ×2	S4 3.707(14)	
						S8 3.193(3) ×2	S6 3.376(4)		

4 Ocna de Fier

Bi1	Bi2	*Me*3	Bi4	*Me*1	*Me*2	Pb3	Pb4	Cu1	Cu2
S9 2.602(6)	S1 2.603(6)	S5 2.696(6)	S8 2.580(6)	S3 2.793(8)	S3 2.721(5) ×2	S9 2.983(4) ×2	S10 2.883(6)	S1 2.353(7) ×2	S4 2.208(14)
S10 2.799(5) ×2	S4 2.718(5) ×2	S7 2.837(5) ×2	S6 2.687(5) ×2	S5 2.900(5) ×2	S3 2.754(8)	S6 3.056(6)	S5 3.002(5) ×2	S3 2.363(14) ×2	S3 2.366(7) ×2
S2 2.843(4) ×2	S2 2.949(4) ×2	S10 3.058(5) ×2	S7 3.036(5) ×2	S8 2.909(5) ×2	S4 2.859(8)	S1 3.150(5) ×2	S9 3.010(4) ×2	S4 3.640(14)	S5 3.249(16)
S7 3.184(6)	S6 3.035(6)	S10 3.450(6)	S2 3.284(6)	S7 3.033(6)	S1 2.893(5) ×2	S8 3.155(5) ×2	S4 3.354(6) ×2	S3 3.642(12) ×2	
						S2 3.166(6)	S6 3.426(7)		

5 Erzwiess

Bi1	Bi2	*Me*3	Bi4	*Me*1	*Me*2	Pb3	Pb4	Ag2	Cu2
S9 2.600(3)	S1 2.608(3)	S5 2.685(3)	S8 2.579(3)	S3 2.752(4)	S3 2.739(2) ×2	S9 2.990(2) ×2	S10 2.894(3)	S3 2.358(6)	S4 2.204(6)
S10 2.800(2) ×2	S4 2.733(2) ×2	S7 2.838(2) ×2	S6 2.696(2) ×2	S8 2.900(2) ×2	S3 2.840(4)	S6 3.055(3)	S5 3.015(2) ×2	S1 2.408(3) ×2	S3 2.378(3) ×2
S2 2.844(2) ×2	S2 2.953(2) ×2	S10 3.063(2) ×2	S7 3.040(2) ×2	S5 2.904(2) ×2	S4 2.849(3)	S1 3.140(2) ×2	S9 3.021(2) ×2	S3 3.610(5) ×2	S5 3.197(7)
S7 3.205(3)	S6 3.026(3)	S10 3.458(3)	S2 3.279(3)	S7 3.022(3)	S1 2.908(2) ×2	S8 3.177(2) ×2	S4 3.344(2) ×2	S4 3.663(6)	
						S2 3.185(3)	S6 3.433(3)		

6 Schareck

Bi1	Bi2	*Me*3	Bi4	*Me*1	*Me*2	Pb3	Pb4	Ag2	Cu2
S9 2.606(4)	S1 2.589(4)	S5 2.699(6)	S8 2.585(4)	S3 2.715(6)	S3 2.707(5) ×2	S9 3.002(4) ×2	S10 2.900(4)	S3 2.344(8)	S4 2.214(9)
S10 2.795(3) ×2	S4 2.719(3) ×2	S7 2.836(3) ×2	S6 2.689(3) ×2	S5 2.871(4) ×2	S4 2.859(5)	S6 3.071(4)	S9 2.991(3) ×2	S1 2.493(4) ×2	S3 2.363(5) ×2
S2 2.843(4) ×2	S2 2.952(4) ×2	S10 3.058(4) ×2	S7 3.028(3) ×2	S8 2.882(3) ×2	S1 2.920(3) ×2	S1 3.115(3) ×2	S5 3.059(4) ×2	S3 3.488(7) ×2	S5 3.059(10)
S7 3.177(4)	S6 3.024(4)	S10 3.455(4)	S2 3.273(6)	S7 3.043(4)	S3 2.932(6)	S2 3.165(6) ×2	S4 3.316(3) ×2	S4 3.687(7)	
						S8 3.206(4) ×2	S6 3.416(5)		

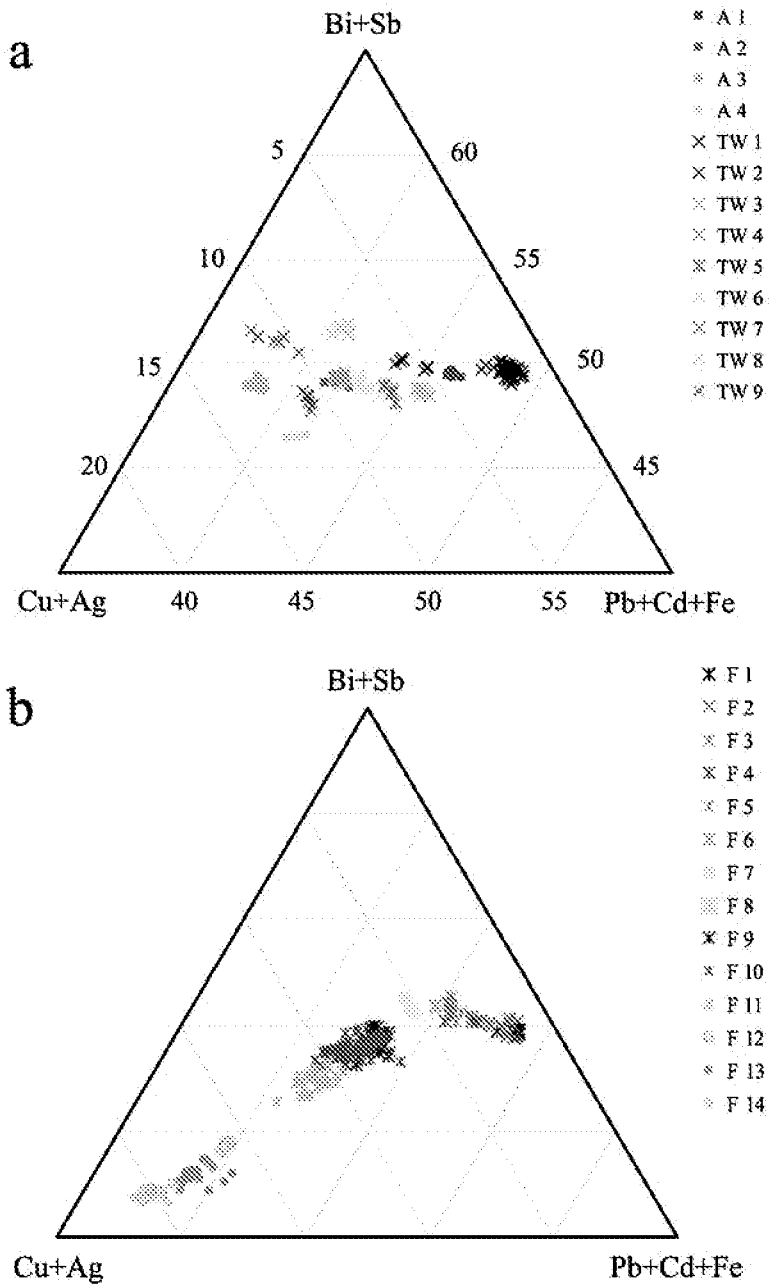

FIG. 1. Cation proportions in the cosalite samples analyzed. All data points were plotted for each sample. Provenance of material: (a–c): Argentina: A; the Alpine deposits: TW: Tauern Window, F: Felbertal deposit, Ff: anomalous Cu-rich rims on grains from the Felbertal deposit. Detailed assignments are in Table 1. (d) Principal averaged data from the literature. The lead-rich cluster was interpreted as a cosalite–galena intergrowth after heyrovskýite.

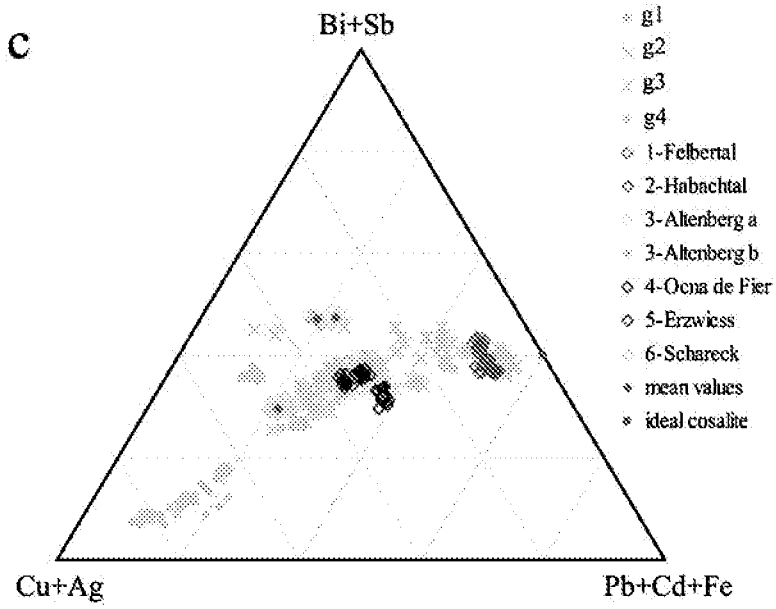

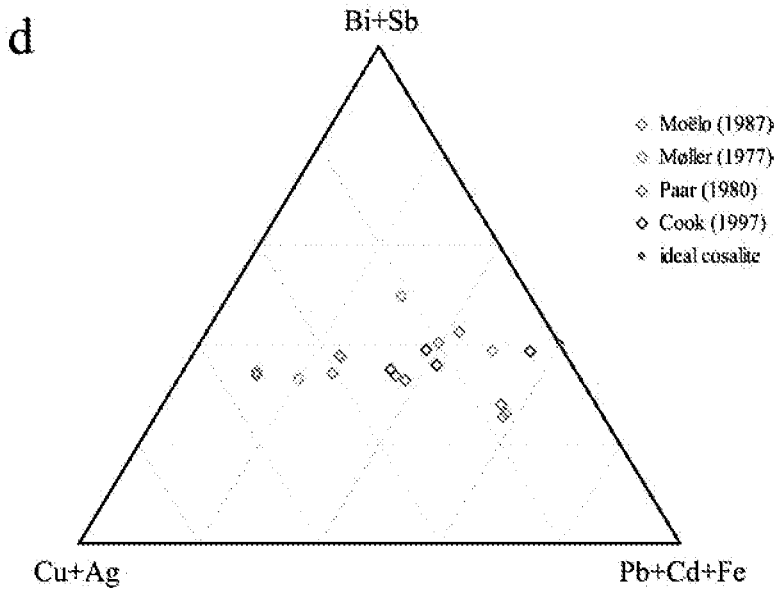

determinations. Using this "excess Bi" also as a measure of *substitutional* Ag replacing Pb according the above equation (Tables 1, 2, formulae), it becomes obvious that a fair amount of silver in cosalite does not follow the Ag + Bi ↔ 2Pb scheme, but takes part in the 2(Cu + Ag*) ↔ Pb* scheme (asterisk denotes the Ag and Pb values "back-corrected" by mathematically eliminating the 2Pb ↔ Ag + Bi substitution; this recalculation is indicated on the diagram as Cu + Ag – Bi^{excess} and Pb + $2Bi^{excess}$ in Fig. 2e). In the formula unit, one half of the (Cu + Ag*) sum "compensates" for the lost Pb values *pfu*, so that the total metal excess over 16 cations *pfu* lags behind the sum of (Cu + Ag*) by a factor of 2 (Fig. 2f).

A linear regression performed on the averaged analytical data (Fig. 4) proves that the incorporation of (Cu + Ag*) proceeds at the expense of Pb*. The regression equation is (Cu + Ag*) *apfu* = 15.58(50) – 1.95(7)

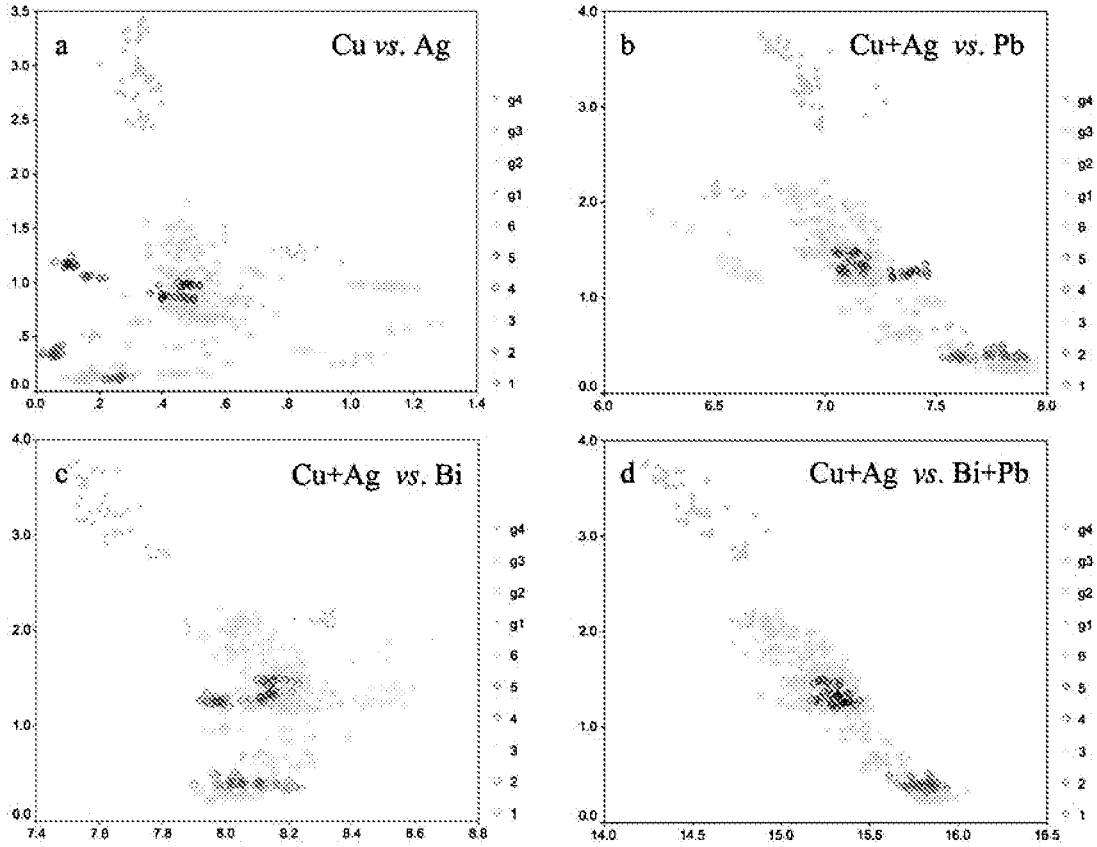

FIG. 2. Correlation diagrams for cations in cosalite, based on a formula unit with 20 anions (*i.e.*, $Pb_8Bi_8S_{20}$). Individual data-points from Tables 1 and 2 are plotted. Colored symbols (1–6) denote the structurally analyzed samples from Figure 1c and Table 2. Grey symbols (g1–g4) represent the chemically analyzed samples from Figures 1a and 1b and Table 1. Explanations of the type *A versus B* relate to elements on the ordinate *versus* the abscissa. Complex element combinations Bi^{excess}, Me^{excess}, Ag_i and Ag_s are explained in the text.

Pb* *apfu*. The standard errors in brackets are given in terms of the last digit, and R^2 is equal to 0.968. For 8 Pb* *apfu*, the calculated value is below 0.02 (Cu + Ag*) *apfu*, whereas for 7 atoms of Pb*, it is 1.96 (Cu + Ag*) *apfu*, with the standard error equal to ~0.03 *apfu*. Therefore, within one standard deviation, the above equation reads $y = 16 - 2x$.

Examination of the distribution of Ag between the portion of silver that participates in the Ag + Bi ↔ 2Pb substitution ("*substitutional* Ag") and that participating in the 2(Cu + Ag)-for-1Pb substitution (all of which we denote here as "*interstitial* Ag" in allusion to its position outside the original cation site, as described further in the structural section) is made difficult by the spread of S values used as a basis of structural formula. This spread projects as a series of negative 1:1 trends overlain on the correlation between the two types of silver in Figures 2g and 2h. It also is visible in, *e.g.*, Figure 2f.

The conservative estimates give silver trends Ag_s/Ag_i between 0:1 and 3:2, *i.e.*, a wide variation, with the samples low in Ag_s having all kinds of Ag_i values, from the lowest to the highest observed (Fig. 2g). The region above the ratio 2:1 is devoid of samples enriched in Ag_s; they cannot be low in Ag_i. The bulk of the Ag_i values are limited to 0.6 *apfu*, with additional scattered points at 0.7–0.8 *apfu*, with a notable exception of a structurally analyzed sample from Schareck, with Ag_i between 1.0 and 1.1 Ag *apfu* (Fig. 2g).

In order to investigate whether the copper and silver concentration in the parent fluids had any influence on the distribution of silver between the Ag_s and Ag_i sites, plots with Ag_s with respect to Ag_i as abscissa, and Ag_i/(Cu + Ag_i) as ordinate were prepared (the former illustrated in Fig. 2h).They show that up to 70%, but with certainty 60% of the interstitial positions can be occupied by silver. This happens both in cosalite with

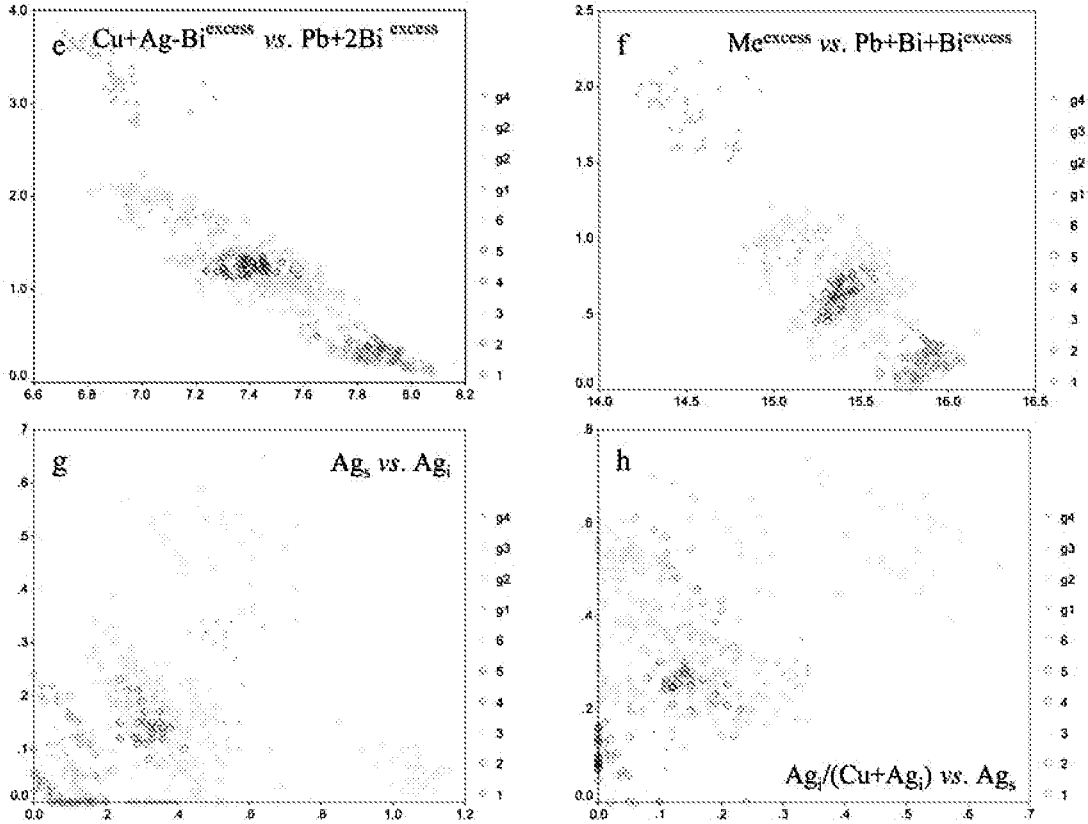

a low total replacement by monovalent cations, *i.e.*, with modest Ag_s and Ag_i values (*e.g.*, no. 1, Felbertal), and in the samples rich in Ag_s (*e.g.*, no. 3a, Altenberg) as well as in the ones with very high values of Ag_i contrasted with very low values of Ag_s (*e.g.*, no. 6, Schareck) (Fig. 2h). For the low to modest values of Ag_s, the entire spectrum of $Ag_i/(Cu + Ag_i)$ values are present. Quite low values of $Ag_i/(Cu + Ag_i)$, however, were not observed in the presence of higher values of Ag_s. Thus, the answer to the above question is negative for most compositions. Are then the high values of Bi or other factors in the mineral association deciding about the part that Ag_s plays in the double role of silver? Data on individual associations are not sufficient to answer this question.

The three substitutional trends for cosalite are summarized in Figure 5. The presence of the Ag + Bi ↔ 2Pb substitution *alone* is not typical for this mineral. On the contrary, the line of the 2(Cu + Ag) ↔ 1Pb substitution in its (nearly) pure form *is* occupied and is flanked by an occupied zone with a mixed character that is parallel to this line. Figure 1 shows that the latter zone consists mostly of individual occurrences that start close to the 2(Cu + Ag) ↔ 1Pb line and branch off in the direction of the Ag + Bi ↔ Pb trend. The Bi-rich boundary for most samples of cosalite is a line running approximately through the Felbertal and Altenberg samples.

As shown in Figure 5, the absolute and relative amount of substitutions can be estimated by defining three (hypothetical) end members: (a) the unsubstituted" $Pb_8Bi_8S_{20}$ composition, *i.e.*, $Pb_{50}Bi_{50}$ in the plot, (b) the hypothetical end-member composition for the Ag + Bi ↔ 2Pb substitution, with four octahedral Pb-containing sites in the above formula fully substituted, *i.e.*, $Ag_2Pb_4Bi_{10}S_{20}$, which plots as $Ag_{12.5}Pb_{25}Bi_{62.5}$ in the diagram (outside the area represented), and (c) the hypothetical end-member for the 2(Cu + Ag) ↔ 1Pb substitution, again with four octahedral Pb-containing sites fully substituted, *i.e.*, $(Cu,Ag)_8Pb_4Bi_8S_{20}$, making $(Cu,Ag)_{40}Pb_{20}Bi_{40}$ in the plot (outside Fig. 5). Molar fractions of these three hypothetical end-members defining a pseudoternary system are m, n and s, respectively, so that $m + n + s = 1$. For a given $(Cu,Ag)_pPb_qBi_r$ composition in Figure 5 ($p + q + r = 100$), $p = 12.5n + 40s$, $q = 50m + 25n + 20s$, and $r = 50m + 62.5n +$

TABLE 7. CHARACTERISTICS OF COORDINATION POLYHEDRA OF CATIONS IN COSALITE FROM SIX LOCALITIES

1	2	3	4	5	6	7	8
1 Felbertal							
Bi1	2.872	0.017	0.300	0.962	99.191	31.047	2.921
Bi2	2.839	0.009	0.238	0.987	95.812	30.216	2.973
*Me*3	3.037	0.069	0.391	0.960	117.354	34.769	2.197
Bi4	2.908	0.017	0.387	0.971	102.992	32.238	2.926
*Me*1	2.925	0.005	0.072	0.999	104.823	33.196	2.171
Ag1	3.048	0.397	0.426	0.310	118.601	22.759	2.068
*Me*2	2.810	0.003	0.119	0.997	92.988	29.498	3.010
Pb3	3.107	0.029	0.104	0.953	125.649	52.897	1.825
Pb4	3.137	0.031	0.295	0.950	129.265	54.312	1.843
Cu1	2.808	0.227	0.754	1.000	92.788	14.828	0.709
Cu2	2.495	0.063	0.731	1.000	65.036	7.463	0.718
2 Habachtal							
Bi1	2.868	0.017	0.301	0.964	98.856	30.945	2.952
Bi2	2.838	0.009	0.233	0.993	95.779	30.223	2.958
*Me*3	3.049	0.075	0.394	0.963	118.675	34.961	2.151
Bi4	2.906	0.016	0.377	0.971	102.779	32.189	2.907
*Me*1	2.929	0.005	0.077	0.997	105.306	33.345	2.146
*Me*2	2.818	0.002	0.105	0.995	93.761	29.782	2.936
Pb3	3.109	0.029	0.107	0.953	125.888	52.996	1.819
Pb4	3.131	0.031	0.300	0.949	128.608	54.010	1.879
Cu1	2.821	0.236	0.752	1.000	94.061	14.867	0.749
Cu2	2.502	0.062	0.807	1.000	65.641	7.543	0.866
3 Altenberg 1							
Bi1	2.873	0.015	0.290	0.973	99.301	31.131	2.887
Bi2	2.832	0.013	0.263	0.976	95.153	29.911	3.087
*Me*3	2.975	0.047	0.390	0.948	110.320	33.480	2.526
Bi4	2.902	0.017	0.394	0.971	102.335	32.030	2.993
*Me*1	2.874	0.004	0.121	0.985	99.404	31.533	2.518
Ag1	2.874	0.004	0.121	0.985	99.404	31.533	0.854
*Me*2	2.827	0.003	0.137	0.988	94.675	30.060	2.890
Pb3	3.099	0.028	0.087	0.954	124.700	52.546	1.846
Pb4	3.126	0.031	0.249	0.940	127.912	53.745	1.843
Ag2	2.827	0.003	0.785	0.988	94.670	30.060	1.610
Cu2	2.462	0.051	0.669	1.000	62.530	7.267	0.896
4 Ocna de Fier							
Bi1	2.859	0.016	0.281	0.971	97.896	30.667	2.975
Bi2	2.831	0.009	0.271	0.995	95.058	30.000	3.087
*Me*3	3.034	0.073	0.383	0.953	117.002	34.537	2.189
Bi4	2.895	0.016	0.377	0.965	101.676	31.841	2.979
*Me*1	2.902	0.003	0.119	0.991	102.355	32.476	2.324
*Me*2	2.805	0.002	0.135	1.000	92.419	29.375	3.061
Pb3	3.101	0.029	0.104	0.961	124.904	52.591	1.850
Pb4	3.123	0.031	0.281	0.949	127.551	53.575	1.894
Cu1	2.804	0.225	0.822	1.000	92.388	14.802	0.801
Cu2	2.470	0.056	0.724	1.000	63.093	7.300	0.923
5 Erzwiess							
Bi1	2.863	0.016	0.290	0.967	98.281	30.787	2.965
Bi2	2.836	0.009	0.262	0.989	95.581	30.165	3.024
*Me*3	3.036	0.070	0.389	0.956	117.202	34.682	2.198
Bi4	2.899	0.015	0.375	0.971	102.006	31.968	2.944
*Me*1	2.891	0.003	0.134	0.997	101.229	32.140	2.403
Ag1	2.891	0.003	0.155	0.997	101.229	32.140	0.836
*Me*2	2.829	0.002	0.124	0.988	94.808	30.132	2.862
Pb3	3.108	0.028	0.101	0.953	125.765	52.966	1.817
Pb4	3.128	0.031	0.271	0.950	128.220	53.858	1.850
Ag2	2.822	0.211	0.795	1.000	94.149	15.367	1.605
Cu2	2.464	0.050	0.699	1.000	62.634	7.291	0.915
6 Schareck							
Bi1	2.856	0.015	0.277	0.970	97.563	30.601	2.981
Bi2	2.828	0.009	0.274	0.989	94.689	29.879	3.119
*Me*3	3.034	0.069	0.383	0.950	116.978	34.677	2.185
Bi4	2.891	0.014	0.371	0.966	101.187	31.757	2.975
*Me*1	2.871	0.001	0.162	0.993	99.137	31.520	2.559
Ag1	2.871	0.001	0.162	0.993	99.137	31.520	0.868
*Me*2	2.840	0.003	0.159	0.956	95.921	30.431	2.834
Pb3	3.111	0.028	0.093	0.948	126.063	53.109	1.798
Pb4	3.125	0.032	0.254	0.943	127.820	53.650	1.850
Ag2	2.817	0.183	0.732	0.999	93.630	15.819	1.437
Cu2	2.438	0.040	0.624	1.000	60.719	7.144	0.937

Coordination numbers are: 6 for Bi1, Bi2, *Me*3, Bi4, *Me*1, Ag1, *Me*2 and Cu1or Ag2, 8 for Pb3, Pb4, and 4 for Cu2. Columns: 1) site label, 2) radius r_s of a circumscribed sphere, least-squares-fitted to the coordination polyhedron, 3) "volume-based" distortion u = [*V*(ideal polyhedron) – *V*(real polyhedron)] / *V*(ideal polyhedron); the ideal polyhedron has the same number of ligands, 4) "volume-based" eccentricity $ECC_V = 1 - [(r_s - \Delta)/r_s]^3$; Δ is the distance between the center of the sphere and the central atom in the polyhedron, 5) "volume-based" sphericity $SPH_V = 1 - 3\sigma_r r_s$; σ_r is the standard deviation of the radius r_s, 6) volume of the circumscribed sphere, 7) volume of the coordination polyhedron, 8) bond-valence sum (Balić-Žunić & Makovicky 1996).

$40s$, which results in $n = (r - q - p/2)/31.25$, $s = (p - 12.5n)/40$, and $m = (q - 25n - 20s)/50$.

For example, the composition $(Cu,Ag)_{10}Pb_{37.5}Bi_{52.5}$, through which the line defining the upper limit of common compositions of cosalite runs in Figure 5, has $p = 10.0$, $q = 37.5$, and $r = 52.5$, which gives $n = 0.32$, $s = 0.15$, and $m = 0.53$ molar fraction of the three end-members defined above, *i.e.*, it is cosalite with almost 50% substitution. In the plot, the points denoted by ***a***, ***b***, ***c***, and ***d*** represent the composition $Ag_{0.5}Pb_7Bi_{8.5}S_{20}$ (containing 75% of the unsubstituted component), $AgPb_6Bi_9S_{20}$, $Cu_2Pb_7Bi_8S_{20}$ (containing 70.6% of the unsubstituted component) and $Cu_4Pb_6Bi_8S_{20}$, respectively.

The substitution trend of the *copper-rich*, oversubstituted cosalite from Felbertal in Figure 5 coincides fully with the substitution line $3Cu^+ \leftrightarrow Bi^{3+}$. Remarkably, it is not positioned on the $Pb_{50}Bi_{50}$ as the origin, but it starts from the point ***c*** on the 2(Cu + Ag) ↔ 1Pb line, at which one Pb atom *pfu* has been replaced by two (Cu + Ag) *apfu*. It was not possible to separate the narrow zones of substitution developed along fractures in cosalite (Fig. 3) for a structure analysis. The location of the extra Cu coming from the $3Cu^+ \leftrightarrow Bi^{3+}$ mechanism of substitution in the structure thus remains unknown. A similar mechanism of substitution ($2Cu^+ \leftrightarrow Fe^{2+}$) was described by Moëlo *et al.* (1984) in jamesonite, as mineral JC, with formula $Cu_2Pb_4Sb_6S_{14}$. It was formed

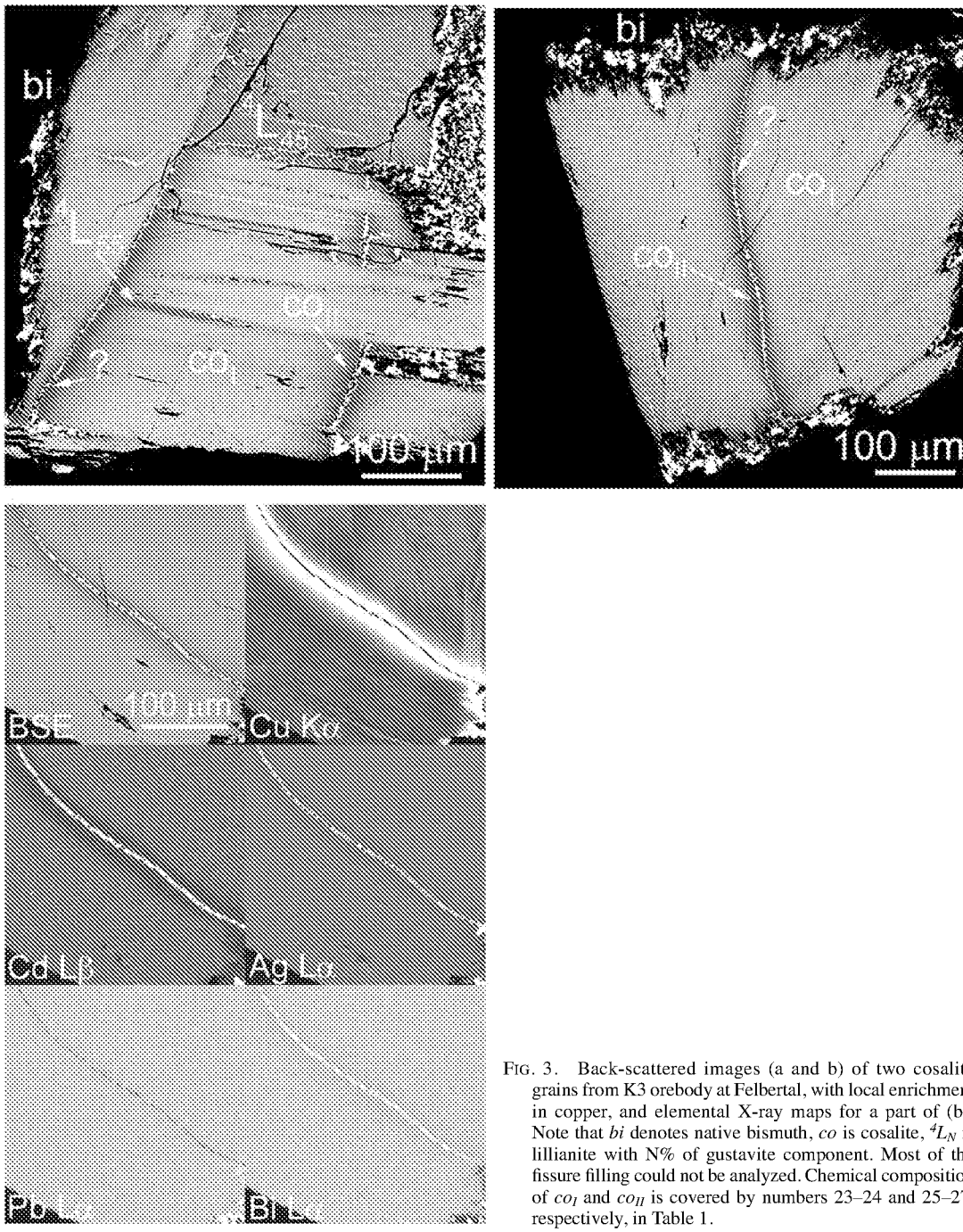

FIG. 3. Back-scattered images (a and b) of two cosalite grains from K3 orebody at Felbertal, with local enrichment in copper, and elemental X-ray maps for a part of (b). Note that *bi* denotes native bismuth, *co* is cosalite, ^4L_N is lillianite with N% of gustavite component. Most of the fissure filling could not be analyzed. Chemical composition of co_I and co_{II} is covered by numbers 23–24 and 25–27, respectively, in Table 1.

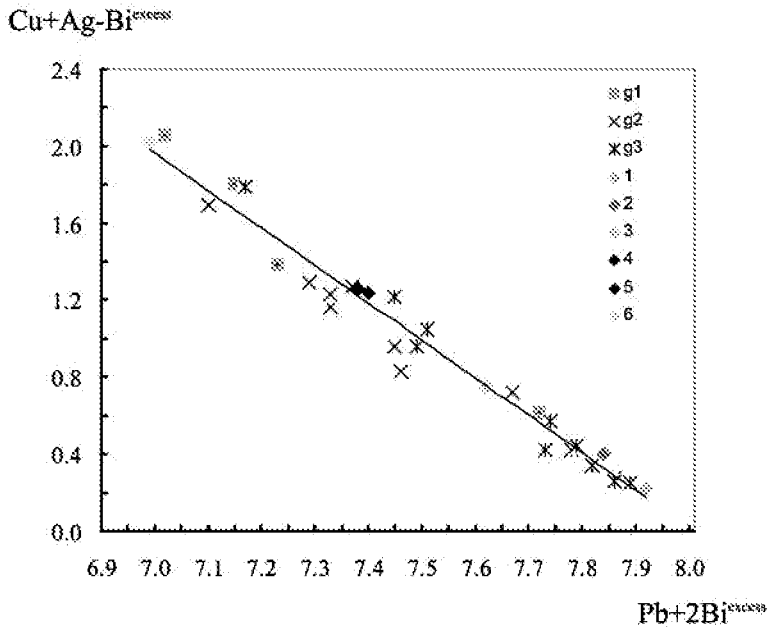

FIG. 4. Correlation between the contents of Cu and Ag in *apfu* not involved in the Ag + Bi substitution and contents of lead that include model Pb obtained by back-correcting the 2Pb → Ag + Bi substitution in the cosalite samples analyzed. For symbols abbreviations, see Figure 1.

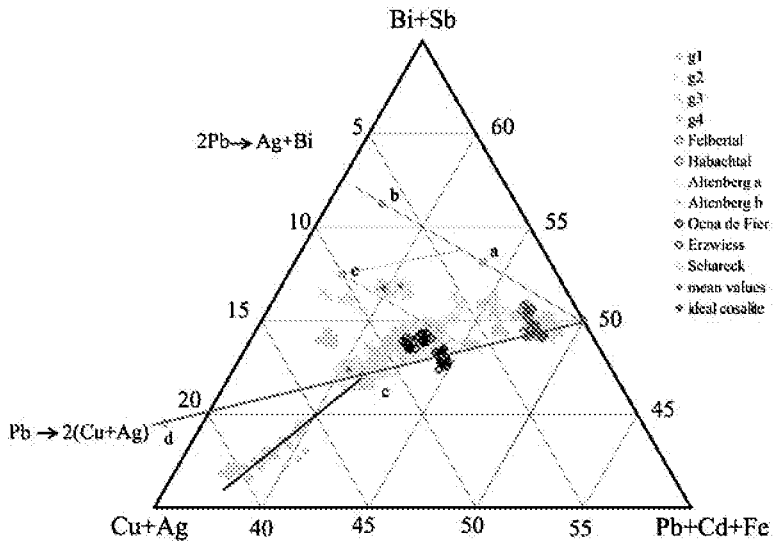

FIG. 5. Cationic compositions of the six structurally analyzed samples of cosalite (colored symbols), as in Figure 1c, with selected trends of substitution indicated. Top red line: pure Ag + Bi → 2Pb substitution starting at $Pb_8Bi_8S_{20}$; bottom red line 2(Cu,Ag) ↔ Pb with the same origin; blue line: 3Cu ↔ Bi substitution starting at the point ***c*** with one Pb atom *apfu* replaced by 2(Cu + Ag). Note that in the last two cases, the amount of cations *pfu* increases as a result of substitution by monovalent elements, which reflects upon their orientation in the plot and a non-linear internal scale. Coordinates of the model point ***e***, $(Ag,Cu)_{10}Pb_{37.5}Bi_{52.5}$, are used to illustrate the position of a cosalite sample in a pseudoternary system composed of two substituted end-members and one unsubstituted end-member.

as a product of metasomatism of the pre-existing sulfosalt by copper-for-iron substitution in the thin surface-layers of the crystals of jamesonite present in tintinaite from Tintina, Yukon.

The unit-cell volume of cosalite drops significantly with the above substitutions, from 1857.8 Å^3 for the sample showing limited substitution to 1830–1837 Å^3 for the most strongly substituted samples. Contributions of the two mechanisms of substitution defined above to this development are not well constrained by the data available.

Crystal Structures

The basic topology

The initial site-notation used in this work follows that used by Srikrishnan & Nowacki (1974). Starting at the octahedral strip site ("Pb2"), Srikrishnan & Nowacki interpreted the inner row of cations as Bi2, Bi1, Bi3, and Bi4, whereas the outer one was labeled trigonal prismatic Pb3 and Pb4, and octahedrally coordinated Pb1. Our structural investigations revealed that it essentially is the Pb1, "Pb2" and Bi3 sites that are influenced by substitutions, and as a consequence, these sites will be designated by us as *Me*1, *Me*2 and *Me*3 (Fig. 6). The detectable Ag + Bi substitution occurs at the site of *Me*1, whereas Cu1 or Ag2 and Cu2 line the walls of the interval of octahedra, *i.e.*, of the *Me*2 coordination polyhedron (Figs. 7, 8). No tetrahedrally coordinated copper, suggested by Srikrishnan & Nowacki (1974), was found.

The crystal structure of cosalite consists of rods of a slightly distorted galena-like structure, parallel to $[110]_{PbS}$, four octahedra wide (octahedra on rod boundaries are modified into square pyramids), and four *Me*–S atomic layers thick (Fig. 7). Most of the outer square pyramids are occupied by Pb, whereas the inner cation positions are preferably occupied by Bi. These rods, oriented diagonally to the (100) plane, are interconnected into (100) layers by intervals of octahedra two octahedra wide (Fig. 7) (Makovicky 1993). The rod surface is alternatively pseudotetragonal in the 100_{PbS} region formed by Pb pyramids and pseudohexagonal, with a hexagonal motif of S atoms on it, in the region of the intervals of octahedra and the adjacent $(111)_{PbS}$ surfaces. Three pseudotetragonal subcells face two orthohexagonal subcells across each interval of the fragmented, zig-zag non-commensurate interface. Bridging this interface, two Pb atoms situated in the pseudotetragonal surface form bicapped trigonal coordination prisms, whereas the last, mixed cation site, designated as *Me*1 below, forms a bridging octahedron.

TABLE. 8. COMPARISON OF THE MODEL COMPOSITION OF ONE UNIT CELL DERIVED FROM THE REFINEMENT OF A CRYSTAL STRUCTURE (str.) WITH THAT DERIVED FROM RESULTS OF AN ELECTRON-MICROPROBE ANALYSIS (chem.)

	chem.	str.		chem.	str.	Ag_i	Ag_s
1) Felbertal			3) Altenberg 1				
S *apfu*	40.00	40.00	S	40.00	40.00		
Cu	0.24	0.53	Cu	0.76	0.81		
Ag	0.52	0.06	Ag	1.72	1.32	0.55	0.77
Pb	15.20	15.28	Sb	1.48	1.79		
Bi	16.32	16.00	Pb	13.26	14.57		
			Bi	15.50	14.21		
2) Habachtal			5) Erzwies				
S *apfu*	40.00	40.00	S	40.00	40.00		
Cu	0.72	1.08	Cu	1.84	1.44		
Ag	0.12	0.00	Ag	0.92	1.23	1.01	0.22
Pb	15.60	15.48	Pb	14.24	14.57		
Bi	16.04	16.00	Bi	16.28	16.00		
4) Ocna de Fier			6) Schareck				
S *apfu*	40.00	40.00	S	40.00	40.00		
Cu	2.28	2.96	Cu	1.94	1.85		
Ag	0.24	0.00	Ag	2.22	2.05	1.73	0.32
Pb	14.76	14.77	Pb	13.74	13.78		
Bi	15.96	16.00	Bi	16.16	16.00		

Substitutional Ag_s and interstitial Cu and Ag_i are defined in the text. Minor amounts of one of the two M^* components could not be reliably refined. Ag_i and Ag_s relate only to samples 3, 5 and 6.

Coordination polyhedra

The series of six determinations of the structure revealed a complex nature of cation substitutions in cosalite. To understand these, a combination of approaches is necessary, consisting of the analysis of structural data (occupancies, displacement factors, bond lengths), and of the empirical chemical formulae based on the results of electron-microprobe analyses, as well as more complex analyses of cation coordinations by means of a hyperbolic relationship between the opposing bond-lengths for elements with pairs of lone electrons (as used by Berlepsch *et al.* 2001a, 2001b), and by calculation of coordination characteristics proposed by Balić-Žunić & Makovicky (1996) and Makovicky & Balić-Žunić (1998), as well as of the bond valences (Brese & O'Keeffe 1991).

These calculations reveal that in the structure of cosalite there are three categories of cation polyhedra: (1) polyhedra not appreciably affected by the substitution and consequent adjustments, (2) polyhedra involved in, and altered during, the process of substitution, and (3) the Cu and Ag* sites, "interstitial" to, and interacting with, the motif of large cation polyhedra (Ag* has been defined above).

The hyperbolic plots (Fig. 9) show that *Bi*2 and *Bi*4, along the pseudohexagonal margin of the PbS-like block, retain their asymmetric coordinations, typical of Bi, virtually unaltered despite all substitutions observed. The same holds for *Bi*1, a more symmetrical Bi site in the block interior, with a conspicuously small difference between the short and longer distances in the

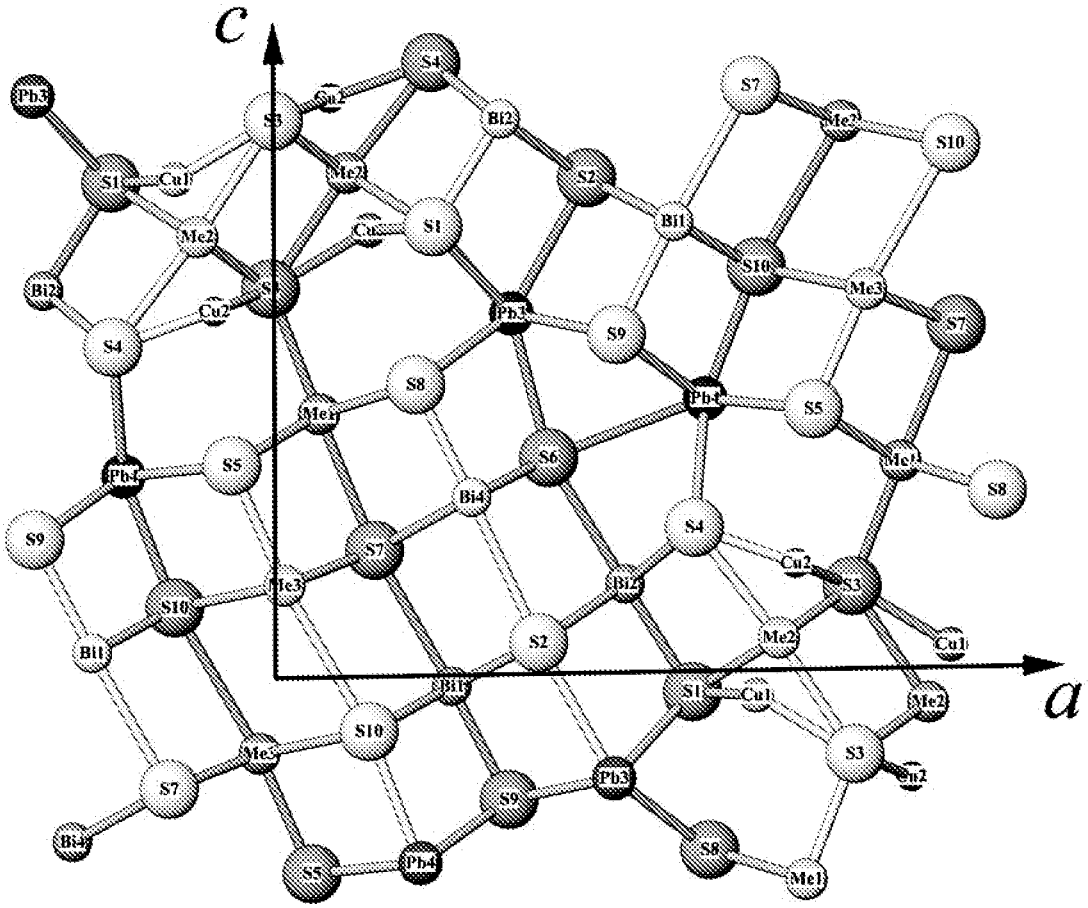

FIG. 6. Site labeling for the cosalite structure. Atoms of Pb are dark blue, cation sites involved in substitutions are light blue, Bi sites are white. Shading indicates sites at two levels of height about 2 Å apart.

base of its coordination pyramid $Bi(S9)(S2)_2(S10)_2$. It is interesting to see how the long Bi–S distances across the lone-electron-pair micelle in the median plane of the rod are influenced by the position of the cation in the elongate micelle: the *Me*3 site has the longest such distance (3.44–3.47 Å). The next longest distances, Bi1–S7 and Bi4–S2, across the median plane of the rod, are a bit reduced in the samples from Ocna de Fier and Schareck, in which the cations are distinguished by extensive substitutions.

The shortest, apical Bi2–S distance is considerably shorter than the hyperbola predicts. It presumably compensates for underbonding of S1 that results from cation substitutions at the nearby *Me*2 site; this distance is shortest for the most strongly substituted samples.

In the Altenberg material, Bi2 and Bi4 are partly replaced by Sb (Table 2); this is reflected in the slightly more asymmetric in-plane configurations of bonds for Bi4, and especially by shorter apical "Bi"–S distances, moving from the Bi hyperbola toward that of Sb, as defined in Berlepsch *et al.* (2001a).

The bicapped trigonal-prismatic positions *Pb*3 and *Pb*4 (Figs. 8, 9) change very little with increasing substitution in cosalite. The coordination polyhedron of Pb3 undergoes shortening of longer Pb–S distances, whereas Pb4 preserves its symmetric configuration.

The bond-length hyperbola for the *Me*3 site situated in the central parts of the PbS-like rod, where the lone-electron-pair micelle is at its broadest, displays bond lengths that are distinctly longer than those of the rest of the Bi sites (Fig. 9). The bonding hyperbola of the *Me*3 site is situated almost halfway between the hyperbola for Bi and the hyperbola for Pb. This indicates a mixed cation site. For all substituted samples, *Me*3 remains on the same bond hyperbola, with the longest Bi–S distance very slightly reduced for the cases of major substitution.

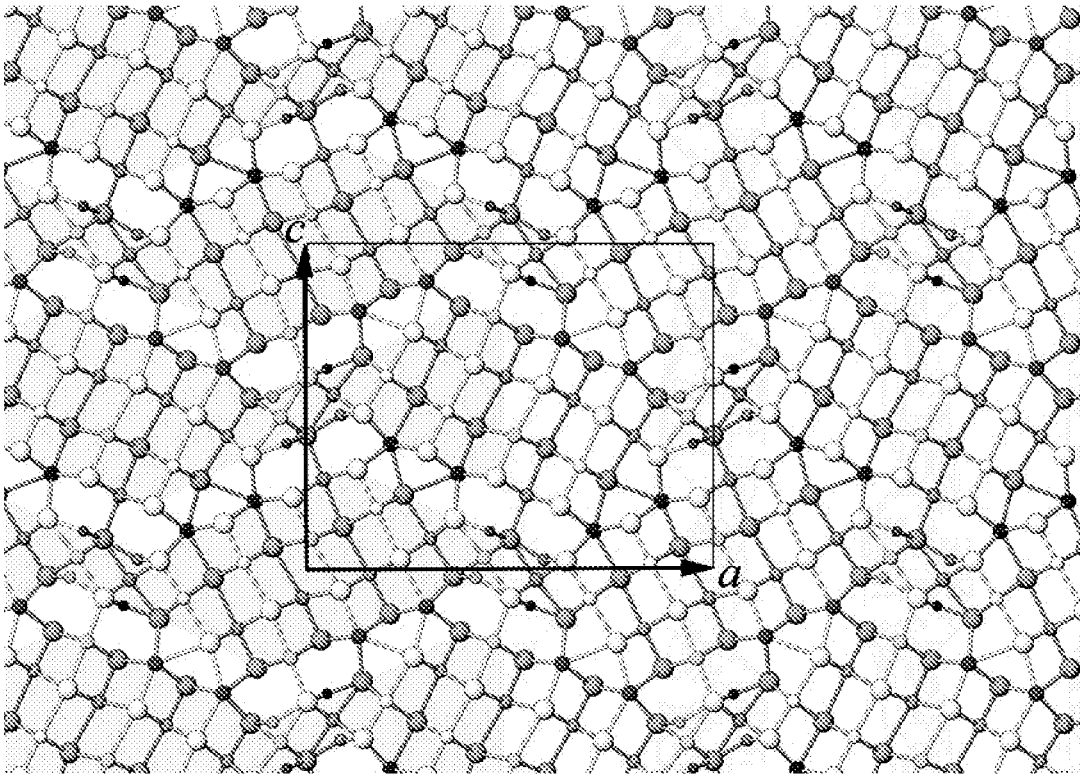

FIG. 7. The crystal structure of cosalite in projection on (010), with atoms at $y = 0.25$ (white) and at 0.75 (grey shading), respectively. In the order of decreasing size, circles represent S, Pb (blue), Bi, a mixed partially occupied position Cu1 or Ag2 or both (green), and Cu2 (red). Rod-layers based on the PbS archetype (Makovicky 1993) are shaded in pink. The right-hand side of the figure shows modules prone to cation substitutions (light blue) between slabs (001) of structure that do not display such substitutions (uncolored).

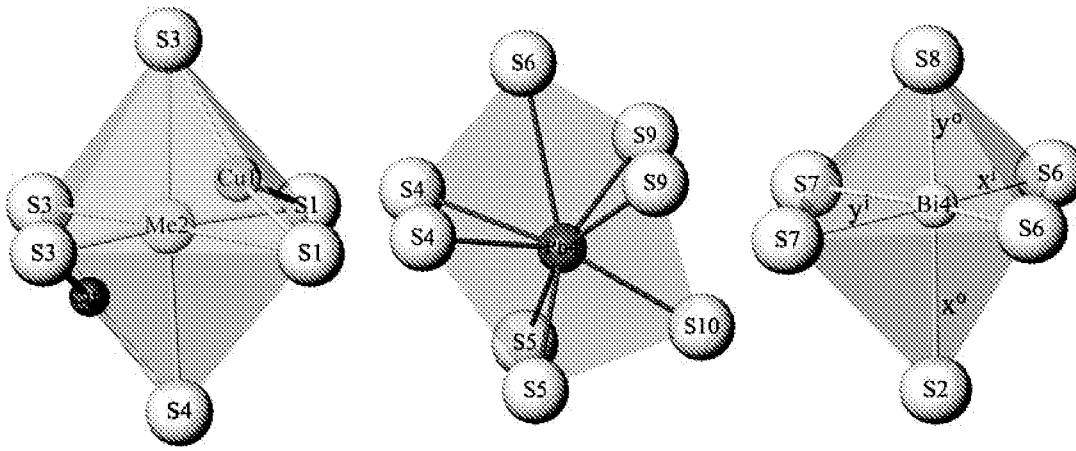

FIG. 8. Coordination polyhedra for Cu1(or Ag2), Cu2, *Me*2, Pb4 and Bi4 in cosalite, and a definition of opposing in-plane (x^i, y^i) and out-of-plane (x^o, y^o) bond pairs in the coordination polyhedra of Bi4.

The only exception is the sample from Altenberg, with important substitution by Cu and Ag at the *Me*1 site, and 20–30% Sb substituting at the Bi2 and Bi4 sites. Here, the in-plane bond ratios for *Me*3 move halfway toward those of pure Bi sites, and the out-of-plane ratios more onto the Bi hyperbola. This trend indicates contents of Bi at the *Me*3 site that are distinctly higher than in the other specimens.

The in-plane values of the bond-length ratios in Figure 9 indicate unambiguously that *Me*2 is a slightly distorted *octahedral Bi site*. The values of the in-plane ratios show that the octahedra are more asymmetric "sideways", in the S1–S3 plane, whereas the out-of-plane S3–Bi–S4 configuration is nearly symmetrical for marginally substituted cosalite. The shape of the *average* octahedron changes in the process of substitution for *Me*2. For a nearly Ag-free situation (Ocna de Fier), the bond distribution follows the Bi hyperbola, but the S3–Bi–S4 bond subset is asymmetric. In the other substituted samples, the configuration S1–Bi–S3 moves below, and the configuration S3–Bi–S4 distinctly above the Bi hyperbola. This trend follows clearly, although in a less symmetric environment, the bond-length ratios observed for Bi octahedra in cuprobismutite homologues (Topa *et al.* 2003b). Here, the slightly foreshortened (*i.e.*, flattened along one axis) octahedra of pure Bi in kupčíkite change to elongate, partly Ag-substituted octahedra in cuprobismutite (with a bond configuration of 2 × 2.854 *versus* 4 × 2.755 Å: Topa *et al.* 2003a). The octahedral distension reaches its maximum for the Schareck sample of cosalite, with the *Me*2–S3 and *Me*2–S4 bonds equal to 2.932 and 2.859 Å, respectively.

Polyhedron characteristics

In the majority of diagrams based on polyhedron volume, volume-based eccentricity or sphericity *versus* degree of substitution (Table 7), the trends connected with Ag1 substitution at the *Me*1 *position* and those for (Ag + Cu) substituting at the *Me*2 *position* are positively correlated in practically all cases, so that they cannot be separated. Therefore, they were replaced by a joint substitution trend expressed in the diagrams as "Ag1

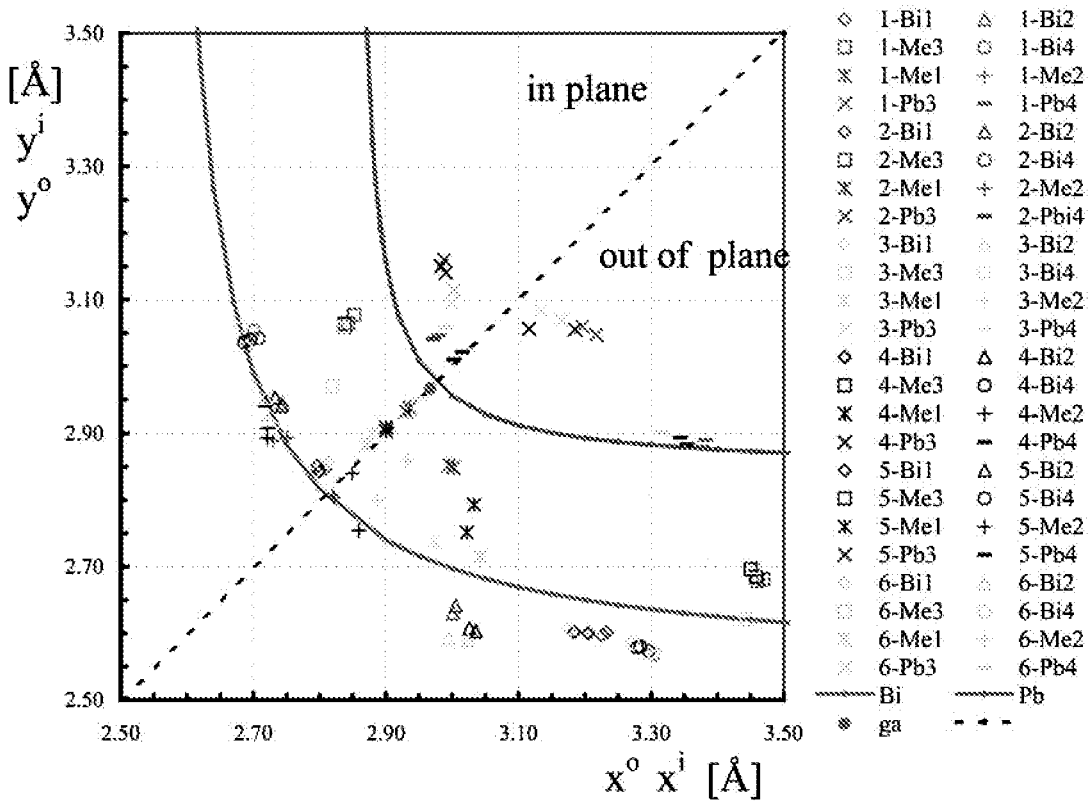

FIG. 9. Hyperbolic relationship of the opposing bond pairs in the coordination polyhedra of Bi, Pb and of the mixed cation positions. Sources of hyperbolae are Topa *et al.* (2003b) for pure Bi, and Berlepsch *et al.* (2001b) for pure Pb, where also a detailed description of the approach is given. First digit in the symbol is the sample number from Tables 2 and 4.

+ (1 – occ."Pb2")". The proof lies in the correlation diagram in Figure 10, where the two above trends combine along a straight line. The Schareck sample has slightly lower Ag substitution than the linear trend predicts, but the Altenberg sample does not follow the linear correlation.

In agreement with a near-constant Bi:Pb ratio at the *Me*3 position of the substituted samples, its $V_{polyhedron}$ changes very little with the degree of substitution (Fig. 11a). However, there is a clear drop in $V_{polyhedra}$ toward the Ocna de Fier sample and a substantial one in the Altenberg sample, both with a high Bi content in this position. A progressive drop in eccentricity (Fig. 11b) is minimal and appears to be connected with overall reduction in the dimension (thickness) of structural rods upon substitution.

The drop in $V_{polyhedron}$ value for the *Me*1 site from the marginally substituted samples toward the substituted ones is due to Bi and Ag + Bi substitution at this site (Fig. 11c). The position of the Altenberg sample expresses ~0.5 "excess Bi" *pfu*, *i.e.*, a marked Ag + Bi substitution at the *Me*1 site.

The eccentricity of the combined *Me*1 position (Fig. 11d) increases regularly with substitution, whereas the opposite holds for volume-based sphericity, which decreases, especially for the substituted Ocna de Fier and Altenberg samples.

The volume of the *Me*2 polyhedron, a pure Bi position according to the bond-relation hyperbolae, is 29.5–29.8 Å^3 in the marginally substituted samples from Felbertal and Habachtal (Fig. 12a). It corresponds to the volumes of unsubstituted Bi octahedra in the members of the cuprobismutite series (Topa *et al.* 2003a, 2003b). It decreases in the Ocna de Fier material, with the Cu:Ag ≈ 10:1 substitution in the *Me*2 octahedra, although not as much as was observed for hodrushite from Swartberg (in which the drop is from 29.6 to 28.7 Å^3). In the course of the substitution by Ag, and by Ag + Cu, this value increases to over 30.4 Å^3, with only slight deviation from linearity (Fig. 12a). Extrapolation to a zero occupancy by Bi leads to the value of at least 31.5 Å^3.

Volume-based eccentricity of the *Me*2 position shows a slight but distinct increase with all substitutions (Fig. 12b). Volume-based sphericity remains close to unity for the degree of total substitution up to 0.35 (Fig. 12c), whereas the volume-based distorsion is lowest for moderately substituted samples (Fig. 12d, Table 7). The rise in $V_{polyhedron}$ of the *Me*2 octahedra with a combined or Ag-rich substitution might be caused either by the increasing steric activity of the lone pair of electrons of Bi in increasingly distorted, asymmetric octahedra, or by incorporation of some Pb instead of Bi, as well as by the distortion of increasingly empty octahedra in the process of accommodating the larger Ag atoms in their walls (as opposed to the smaller Cu).

In order to gain an overall picture of the polyhedron changes connected with the substitution processes, *all cation sites* with distorted-octahedron coordination in the cosalite samples studied were plotted in Figure 13. The increase in eccentricity of the Bi2 site with substitution is paralleled by a decrease of this value for Bi1

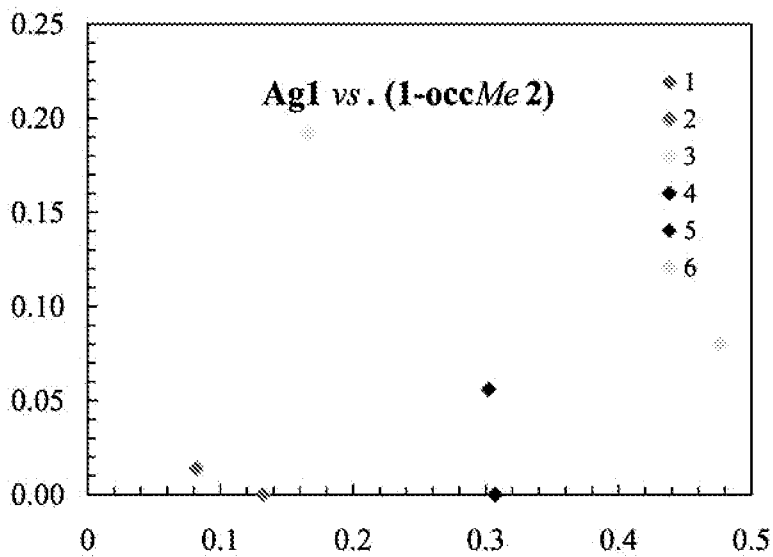

FIG. 10. Correlations between the contents of Ag1 in the position *Me*1 and the amount of vacancies in the central *Me*2 cation (accompanied by insertion of Cu and Ag in its periphery) in the structurally analyzed samples of cosalite.

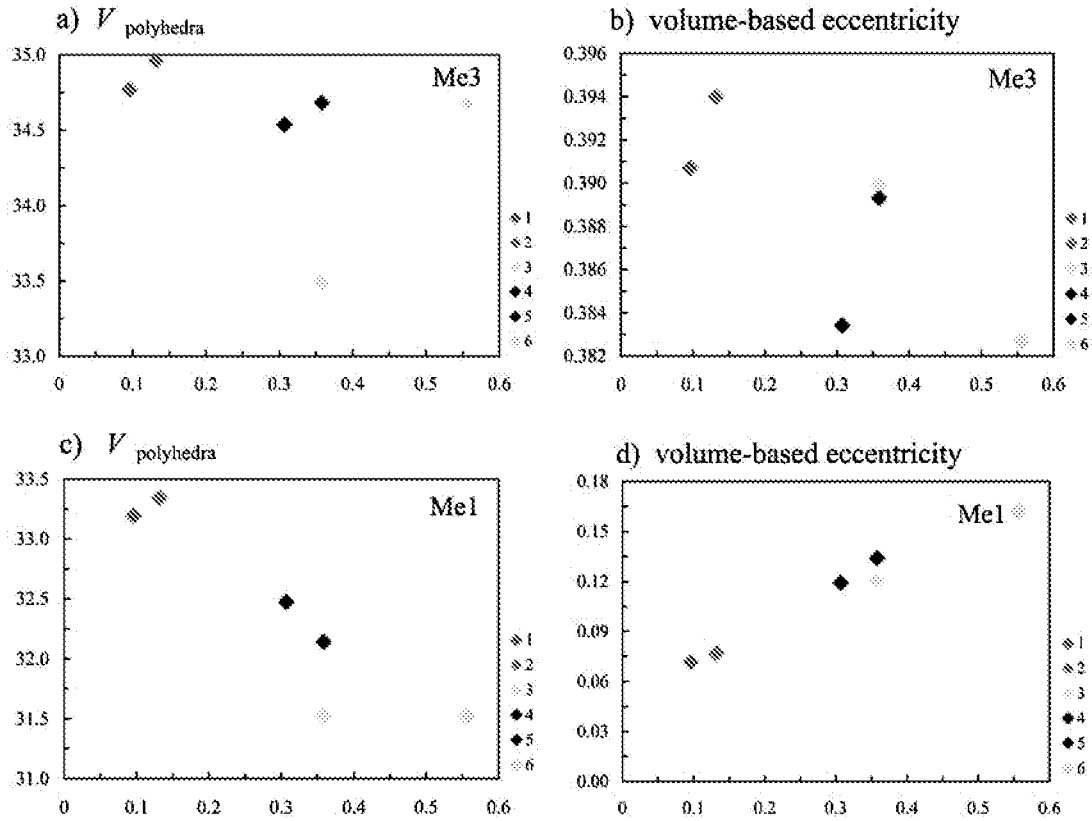

FIG. 11. Correlation between a polyhedron volume and a measure of volume-based eccentricity, respectively, for the *Me*1 and Bi3 sites, and the combined substitution in the *Me*1 and *Me*2 sites in cosalite (*i.e.*, occupancy of Ag1 + [1 – occupancy of *Me*2]).

and Bi4 (and, in part, by *Me*3 as well). The behavior of the Bi2 site might be connected with the increasing underbonding of those sulfur atoms that are shared with the *Me*2 site. The combined substitutions in the *Me*1 site lead to a markedly increasing eccentricity. The composite trend for the *Me*2 site has already been mentioned.

The mechanism of substitution

The process of substitution *compositionally* means replacement of Pb by Ag + Cu; the principal *structural* feature, however, besides some degree of "lillianite-like" substitution, Ag + Bi ↔ 2Pb), is the replacement of a distinct Bi site by Ag + Cu in the walls of its polyhedron, and this calls for explanation. One of our findings is the realization that the solution of this apparent contradiction lies in preservation of a local balance of valences, similar to the case of other sulfosalts with complex substitutions, *e.g.*, those belonging to the cuprobismutite family (Topa *et al.* 2003b).

Figure 14 summarizes the principal features of the processes involved. All of them are plotted against the percentage of vacancies created at the octahedral *Me*2 site, which can be up to about half-empty. The apparent bond-valence sum for Bi at this site drops from over 3 to almost 2.8 in the process, but we consider this information an artefact arising from the slow expansion of the *Me*2 polyhedron while being progressively vacated. A real trend, however, is the increase of the bond-valence sum at the *Me*1 site, from close to 2.1 to almost 2.6, indicating increasing Bi contents in the site, not compensated by an equivalent amount of silver, which is shown at the top of Figure 14. The bond-valence sum for the *Me*3 site, a mixed Pb,Bi site (Wulf 1988, 1995), is remarkably constant, just below 2.2, notwithstanding the amount and type of substitutions at the sites *Me*2 (and the Cu,Ag sites flanking it) and *Me*1. Finally, the combined occupancy of the two

Cu and Ag sites flanking the vacated *Me*2 site shows a close-to-linear relationship with the amount of vacancies at the *Me*2 site.

Aberrations are few: Bi at *Me*2 of the sample from Ocna de Fier appears to have a bond-valence sum exceeding 3 *vu* because the Cu–S bonds in the copper-flanked *Me*2 octahedron contract it in comparison to a fully occupied one. The sample is poor in Ag, also at the *Me*1 site, and this is compensated by augmented Cu occupancy of the sites flanking *Me*2. The Altenberg sample, rich in Ag, has high Bi contents at both *Me*1 and *Me*3, judging from the bond-valence sums. It also is rich in Ag entering the *Me*1 site.

In total, *the principal mechanism of substitution in cosalite* consists of the progressive creation of vacancies at the *Me*2 site (a Bi site), with 2/3 of the charge deficit thus created compensated by the flanking triangular – flat pyramidal Cu and Ag sites. The remaining deficit, which causes underbonding, especially at the S3 positions, is compensated primarily by introduction of Bi at the *Me*1 sites, uncompensated by equivalent amounts of Ag. These are bonded directly to S3. The small amounts of Ag at the *Me*1 site (presumably compensated by an appropriate portion of Bi) increase with degree of substitution, reaching up to 6–9 at.%, whereas about 20 at.% of Bi present in the Pb-based *Me*3 site remains approximately constant (as obtained from bond-valence sums). Thus, these two mechanisms do not play an important role in charge compensation. This combination of parallel processes of omission, interstitial insertion and substitution leads to the resulting effect of (Cu + Ag) substituting for lead in the chemical formula of cosalite.

Summary of Individual Substitutions

An analysis of polyhedron attributes reveals that:

(1) the "*Me*2" site is a partly vacant, distorted octahedral site containing bismuth, in agreement with the original suggestion by Macíček (1986). Vacancies

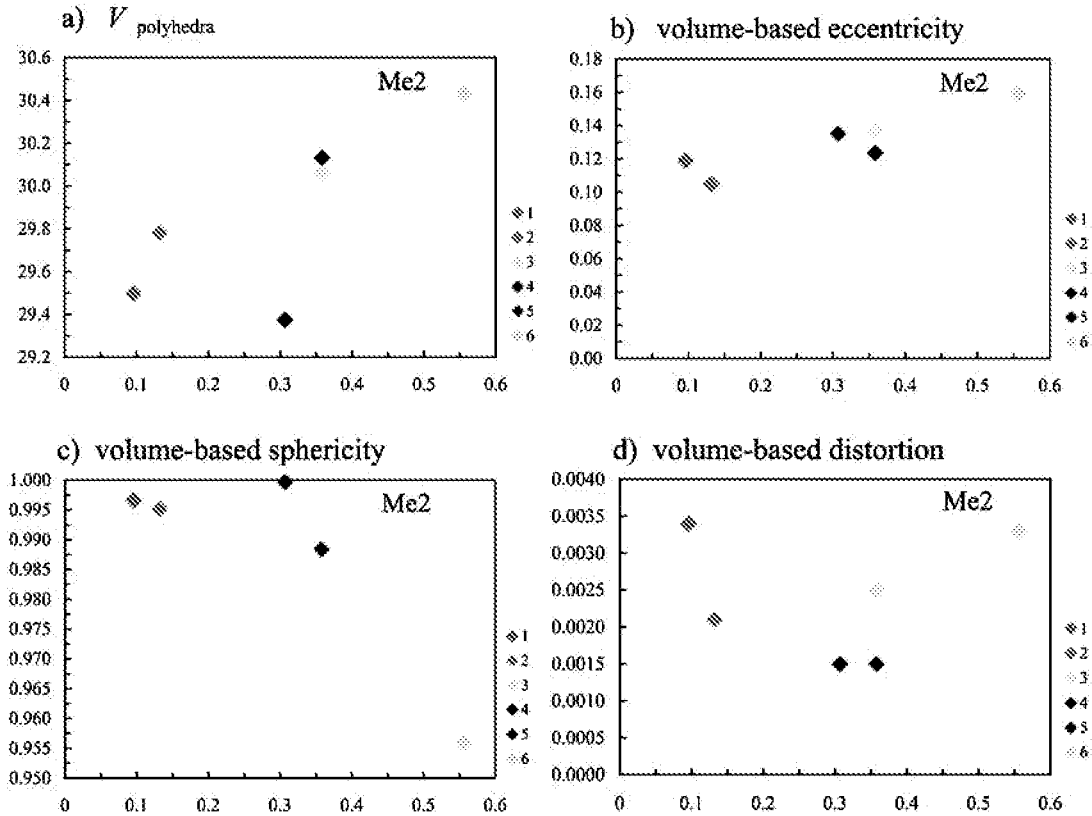

FIG. 12. Correlation between the polyhedron characteristics of the *Me*2 site and the combined substitution at the *Me*1 and *Me*2 sites in cosalite, as defined in Figure 4. Diagrams (a–d): a) polyhedron volume, b) volume-based eccentricity, c) volume-based sphericity and d) volume-based distortion index (for definitions, see Table 7). In Figure 12c, points numbers 3 and 5 coincide.

are accompanied by occupancy of the opposing, "free" octahedron walls by Cu1, Cu2 and (Ag2), all in three-fold coordination.

(2) Considering all the evidence, this occupancy is statistical, but with a strong preference of silver for a slightly pyramidal Cu site over the trigonal planar site. Dimensions of the "*Me*2" site deviate progressively from those characteristic for Bi as the degree of Ag substitution increases.

(3) The *Me*3 site appears to be a mixed site with a fairly constant Pb:Bi ratio, except for the case of the Altenberg sample, which displays a very high degree of the overall Bi + Ag → 2Pb substitution. In this case, the *Me*3 site appears to have accommodated a higher proportion of Bi.

(4) The *Me*1 position appears to be a mixed position, even in the samples with a low degree of substitution; there it displays a preponderance of Pb. It manifests a considerable and increasing degree of substitution in all samples of substituted cosalite. It appears to absorb especially much Bi in the Ag-rich sample from Altenberg. The bond-valence values confirm that there are important Bi contents present at the *Me*1 site that are not matched by Ag contents.

(5) The remaining cation sites, Bi1, Bi2, Bi4, Pb3, and Pb4, are only marginally influenced by the substitution processes. They adjust slightly to the geometry and size of the substituted polyhedra and of the resulting structure.

(6) In the structure of cosalite, the measurable substitutions are limited to one-to-two octahedra thick slabs [(100) in our orientation] with a periodically changing thickness. They are spaced *a*/2 apart and alternate with slabs two octahedra thick, in which there is little or no change (Fig. 7). The substitutions located in the substitution-prone slabs are cross-correlated in order to maintain a local balance of valences and to maintain a size coherence of all substituted and unsubstituted polyhedra.

(7) Spanning two consecutive *Me*2 pairs in the structure is a row of substituted *Me*2–*Me*1–*Me*3–*Me*3–*Me*1–*Me*2 sites. These planar segments are glide-planes related to a similar system of plane segments at *c*/2 (our orientation). Together they, or a similar type of

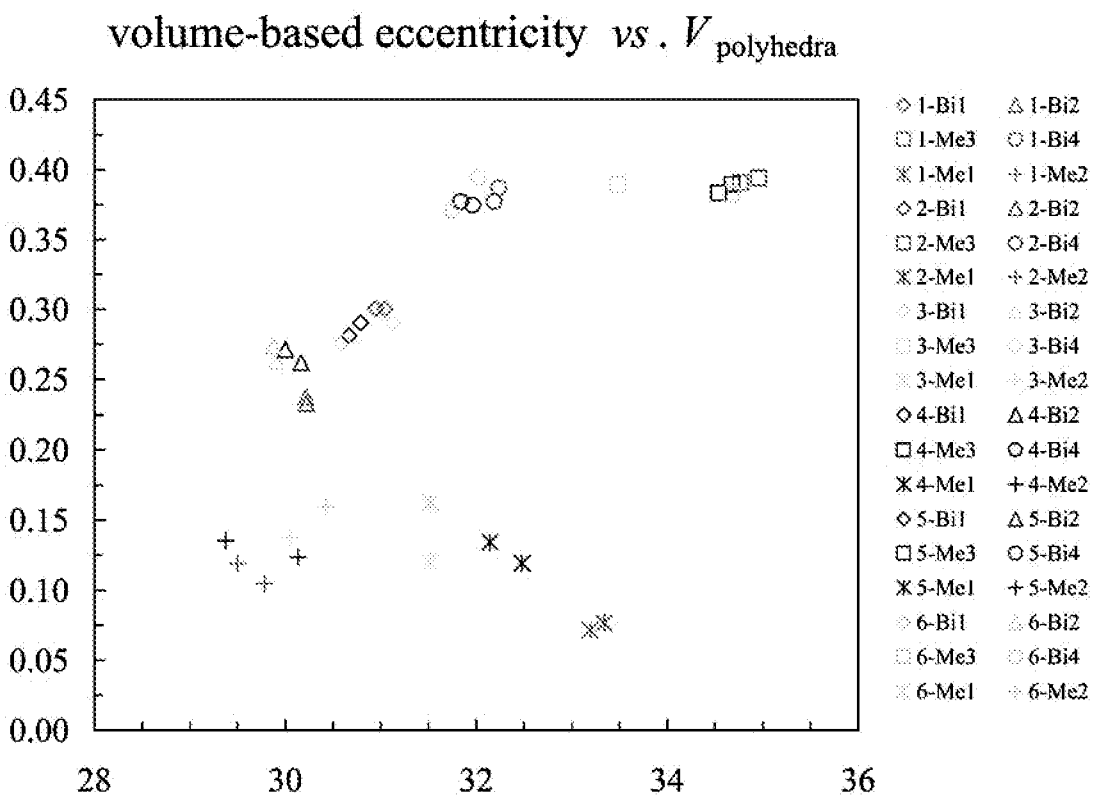

FIG. 13. Volume-based eccentricity plotted against polyhedron volume of the distorted coordination octahedron in the cosalite structures examined. The Bi1, 2 and 4 sites are pure Bi sites, *Me*1–3 are mixed sites.

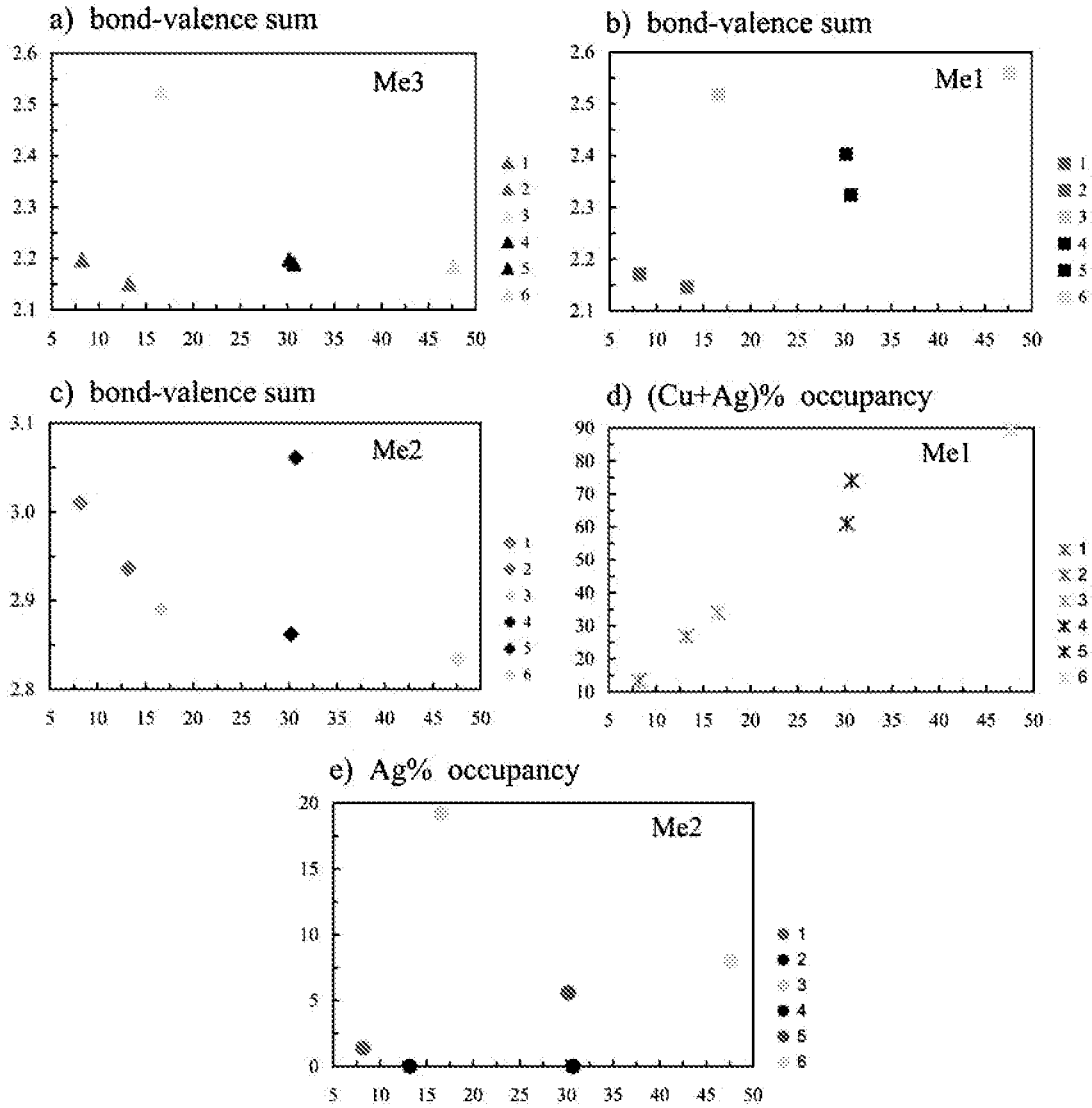

FIG. 14. Individual components of the substitution process in cosalite. All changes are plotted against the percentage of vacancies at the *Me*2 position. (a) Bond-valence sum for the *Me*3 site, (b) bond-valence sum for the *Me*1 site, (c) (apparent) bond-valence sum for the progressively vacated *Me*2 site, (d) the compound (Cu + Ag) occupancy of the two triangular faces of the *Me*2 coordination octahedron, and (e) occupancy of Ag at the *Me*1 site; both latter values come from the structure refinements (in %). For color codes, see Figure 2.

modulation, might be responsible for the satellite reflections observed by Pring & Etschmann (2002) using electron diffraction. The orientation of the substituted planes and that of the reciprocal lattice rows defined by satellites agree perfectly. As already stated by the original authors, only the first-order satellites have considerable intensities; their spacing should indicate a ~2*c* modulation, at variance with the situation observed in our samples.

(8) The single sample of cosalite with appreciable antimony contents analyzed by us indicates that Sb prefers the marginal bismuth sites Bi2 and Bi4. For these sites, the dimensions of the lone-electron-pair micelle are easy to adjust in an environment dominated by the longest Pb4–S distances. The surrounding polyhedra of Pb can adjust to the smaller SbS_5 coordination pyramid as well.

(9) The combination of chemical and structural data elucidates the complex mechanism of substitution in cosalite, as was summarized in the previous section. Because of the multiple sites involved in the substitution and mutually coupled mechanisms of substitution, the composition of cosalite is one of the most complicated among the Pb–Bi sulfosalts. On the basis of the chemical data alone, it can be expressed as percentages of the three hypothetical end-members, the "unsubstituted" one and two substituted ones. No variations in the contents of sulfur in the unit cell, assumed in the formula proposed by Mozgova & Bortnikov (1980), were found.

(10) The general structural formula for cosalite can be expressed as: $Cu_xAg_{i+s}Pb_{8-2s-0.5(x+i)}Bi_{8+s}S_{20}$. The subscript s denotes the quantity of Ag and Bi in *apfu* substituting for Pb, whereas x and i denote the quantity of Cu and Ag in *apfu*, respectively, that compensate in part for the vacated *Me*2 position.

Acknowledgements

We thank Prof. Dr. W.H. Paar and Drs. H. Putz, E. Kirchner, and G. Ilinca for samples of ore material, which turned out to contain cosalite suitable for structure determination. Dan Topa thanks to Dr. T. Balić-Žunić for introduction to the practice of X-ray crystallography ten years ago, in 1999, for which material from Felbertal was used. DT gratefully acknowledges the support of the Christian Doppler Research Society (Austria). EM was supported by grant no. 272–08–0227 of the Research Council for Nature and Universe (Denmark). We thank Drs. Nadia Mozgova and Nigel Cook for constructive reviews, and Prof. Robert F. Martin for a thoughtful review and editorial assistance.

References

Balić-Žunić, T. & Makovicky, E. (1996): Determination of the centroid or 'the best centre' of a coordination polyhedron. *Acta Crystallogr.* **B52**, 78-81.

Balić-Žunić, T. & Vicković, I. (1996): IVTON – program for the calculation of geometrical aspects of crystal structures and some crystal chemical applications. *J. Appl. Crystallogr.* **29**, 305-306.

Berlepsch, P., Makovicky, E. & Balić-Žunić, T. (2001a) Crystal chemistry of meneghinite homologues and related sulfosalts. *Neues Jahrb. Mineral., Monatsh.*, 115-135.

Berlepsch, P., Makovicky, E. & Balić-Žunić, T. (2001b): Crystal chemistry of sartorite homologues and related sulfosalts. *Neues Jahrb. Mineral., Abh.* **176**, 45-66.

Berry, L.G. (1939): Studies of mineral sulpho-salts. 1. Cosalite from Canada and Sweden. *Univ. Toronto Studies, Geol. Ser.*, 23-30.

Brese, N.E. & O'Keeffe, M. (1991): Bond-valence parameters for solids. *Acta Crystallogr.* **B47**, 192-197.

Bruker AXS (1998a): SMART, Version 5.0, Bruker AXS, Inc., Madison, Wisconsin 53719, USA.

Bruker AXS (1998b): SAINT, Version 5.0, Bruker AXS, Inc., Madison,Wisconsin 53719, USA.

Bruker AXS (1998c): XPREP, Version 5.1, Bruker AXS, Inc., Madison,Wisconsin 53719, USA.

Ciobanu, C.L., Cook, N.J., Pring, A., Brugger, J., Danyushevsky, L.V. & Shimizu, M. (2009): "Invisible gold" in bismuth chalcogenides. *Geochim. Cosmochim. Acta* **73**, 1970-1999.

Cook, N.J. (1997): Bismuth and bismuth–antimony sulphosalts from Neogene vein mineralisation, Baia Borsa area, Maramures, Romania. *Mineral. Mag.* **61**, 387-409.

Genth, F.A. (1885): Contributions from the Laboratory of the University of Pensylvania. XXIV. Contributions to Mineralogy. 5. Cosalite. *Proc. Am. Philosoph. Soc.* **23**, 36-37.

Karup-Møller, S. (1977): Mineralogy of some Ag–(Cu)–Pb–Bi sulphide associations. *Bull. Geol. Soc. Denmark* **26**, 41-68.

Lee, C.H. & Park, H.I. (1995): Some Pb–Bi–Sb–S minerals from the Dunjeon gold mine, northern Taebaegsan mining district, Korea. *Resource Geology* **45**, 323-329.

Lee, C.H., Park, H.I. & Chang, L.L.Y. (1993): Sb-cosalite from Dunjeon gold mine, Taebaeg City, Korea. *Mineral. Mag.* **57**, 527-530.

Macíček, J. (1986): The crystal chemistry of cosalite. *Collected Abstr., Xth Eur. Crystallogr. Meeting (Wroclaw)*, 260.

Makovicky, E. (1981): The building principles and classification of bismuth–lead sulphosalts and related compounds. *Fortschr. Mineral.* **59**, 137-190.

Makovicky, E. (1989): Modular classification of sulphosalts – current status. Definition and application of homologous series. *Neues Jahrb. Mineral., Abh.* **160**, 269-297.

Makovicky, E. (1993): Rod-based sulphosalt structures derived from the SnS and PbS archetypes. *Eur. J. Mineral.* **5**, 545-591.

Makovicky, E. & Balić-Žunić, T. (1998): New measure of distortion for coordination polyhedra. *Acta Crystallogr.* **B54**, 766-773.

Moëlo, Y., Jambor, J.L. & Harris, D.C. (1984): Tintinaïte et sulfosels associés de Tintina (Yukon): la cristallochimie de la série de la kobellite. *Can. Mineral.* **22**, 219-226.

Moëlo, Y., Marcoux, E., Makovicky, E., Karup-Møller, S. & Legendre, O. (1987): Homologues de la lillianite

(gustavite, vikingite, heyrovskyite riche en Ag, Bi ...) de l'indice à W–As–(Pb,Bi,Ag) de La-Roche-Balue (Loire-Atlantique, France). *Bull. Minéral.* **110**, 43-64.

MOËLO, Y., MAKOVICKY, E., MOZGOVA, N.N., JAMBOR, J.L., COOK, N., PRING, A., PAAR, W.H., NICKEL, E.H., GRAESER, S., KARUP-MØLLER, S., BALIĆ-ŽUNIĆ, T., MUMME, W.G., VURRO, F., TOPA, D., BINDI, L., BENTE, K. & SHIMIZU, M. (2008): Sulfosalt systematics: a review. Report of the sulfosalt sub-committee of the IMA Commission on Ore Mineralogy. *Eur. J. Mineral.* **20**, 7-46.

MOZGOVA, N.N. & BORTNIKOV, N.S. (1980): *Sulfosalts, Platinum Minerals and Ore Microscopy*. Nauka, Moscow, Russia (31- 49).

MOZGOVA, N.N., NENASHEVA, S.N., EFIMOV, A.V., BORODAEV, Y.S. & MOËLO, Y. (1992): Wittite with Se-rich cosalite and bismuthinite from Nevskoye tin deposit (Magadan district, Russia). *Mineral. Petrol.* **46**, 137-153.

PAAR, W.H., CHEN, T.T., MEIXNER, H. (1980): Pb–Bi–(Cu)-sulfosalts in Paleozoic gneisses and schists from Oberpinzgau, Salzburg Province, Austria. *Tschermaks Mineral. Petrogr. Mitt.* **27**, 1-16.

PALACHE, C., BERMAN, H. & FRONDEL, C. (1966): *The System of Mineralogy*. 1. *Elements, Sulfides, Sulfosalts*. John Wiley & Sons, Inc., New York, N.Y.

PRING, A. & ETSCHMANN, B. (2002): HRTEM observations of structural and chemical modulations in cosalite and its relationship to the lillianite homologues. *Mineral. Mag.* **66**, 451-458.

SHELDRICK, G.M. (1997a): SHELXS–97. A *Computer Program for Crystal Structure Determination*. University of Göttingen, Göttingen, Germany.

SHELDRICK, G.M. (1997b): SHELXL–97. *A Computer Program for Crystal Structure Refinement*. University of Göttingen, Göttingen, Germany.

SKOWRON, A. & BROWN, I.D. (1990): Structure of antimony lead selenide, $Pb_4Sb_4Se_{10}$, a selenium analog of cosalite. *Acta Crystallogr.* **C46**, 2287-2291.

SRIKRISHNAN, T. & NOWACKI, W. (1974): A re-determination of the crystal structure of cosalite, $Pb_2Bi_2S_5$. *Z. Kristallogr.* **140**, 114-136.

SUGAKI, A., KITAKAZE, A. & SHIMA, H. (1982): Synthesis of cosalite and its phase relations in the Cu–Pb–Bi–S quaternary system. *In* Crystal Chemistry of Minerals (S.J. Mincheva, ed.). Proc. 13th General Meeting **1**. Int. Mineral. Assoc. (Varna), E. Sweizerbartsche Verlagsbuchhandlung, Stuttgart, Germany (291-298).

TOPA, D. (2001): *Mineralogy, Crystal Structure and Crystal Chemistry of the Bismuthinite–Aikinite Series from Felbertal, Austria*. Ph.D. thesis, Institute of Mineralogy, Univ. Salzburg, Salzburg, Austria.

TOPA, D., MAKOVICKY, E. & BALIĆ-ŽUNIĆ, T. (2003b): Crystal structures and crystal chemistry of members of the cuprobismutite homologous series of sulfosalts. *Can. Mineral.* **41**, 1481-1501.

TOPA, D., MAKOVICKY, E., BALIĆ-ŽUNIĆ, T. & PAAR, W.H. (2003a): Kupčíkite, $Cu_{3.4}Fe_{0.6}Bi_5S_{10}$, a new Cu–Bi sulfosalt from Felbertal, Austria, and its crystal structure. *Can. Mineral.* **41**, 1155-1166.

TOPA, D., MAKOVICKY, E., PAAR, W.H. & BALIĆ-ŽUNIĆ, T. (2001): Felbertalite, $Cu_2Pb_6Bi_8S_{19}$, a new mineral species from Felbertal, Salzburg Province, Austria. *Eur. J. Mineral.* **13**, 961-972.

WEITZ, G. & HELLNER, E. (1960): Über komplex zusammengestzte sulfidische Erze. VII. Zur Kristallstruktur des Cosalits, $Pb_2Bi_2S_5$. *Z. Kristallogr.* **113**, 385-402.

WULF, R. (1988): Experimental-determination of Pb/Bi distribution in complex sulfide compounds. *Z. Kristallogr.* **182**, 267-269.

WULF, R. (1995): Experimental distinction of elements with similar atomic-number in (Pb,Bi)-sulfosalts. *Mineral. Petrol.* **52**, 187-196.

Received November 12, 2009, revised manusript accepted September 20, 2010.